Doctoral Dissertation

The Role of $[Ca^{2+}]_i$ Fluctuation in Cortical Neural Progenitor Cells

Putu Adi Andhika Rhaditya

Graduate School of Brain Science, Doshisha University

A thesis submitted for the degree of

Doctor of philosophy in science

Date 28-11-2022

Abstract

Fluctuations in intracellular calcium ($[Ca^{2+}]_i$) levels are involved in various processes during the development of the central nervous system, such as in the proliferation of neural progenitor cells (NPCs) and in the migration of immature neurons from the ventricular zone (VZ) to the cortical plate. However, the roles of $[Ca^{2+}]_i$ fluctuations in NPC development, especially in the differentiation of self-renewing NPCs into neuron-generating NPCs and immature neurons, have not been elucidated. Here, we performed calcium imaging of acute cortical slices and cells isolated from the mouse embryonic cortex to examine temporal changes in $[Ca^{2+}]_i$ fluctuation patterns in VZ cells from E12 to E16. We observed that at E11, Pax6-positive NPCs and Tuj1-positive immature neurons exhibited distinct $[Ca^{2+}]_i$ fluctuations, with transient $[Ca^{2+}]_i$ fluctuations observed in numerous immature neurons compared to only a few Pax6-positive NPCs, suggesting that the change in $[Ca^{2+}]_i$ fluctuation patterns correlates with their differentiation. The $[Ca^{2+}]_i$ fluctuation during NPC development was mediated primarily by the T-type calcium channel, and blocking this calcium channel in neurosphere cultures increased the number of spheres and inhibited neuronal differentiation. Consistently, *in vivo* knockdown of T-type calcium channels subtype, Cav3.1 by RNAi maintained the Pax6-positive cells as self-renewing NPCs while simultaneously suppressing their neuronal differentiation into immature neurons. These results reveal that $[Ca^{2+}]_i$ fluctuations mediated by Cav3.1 are required for the neural differentiation of Pax6-positive self-renewing NPCs.

Acknowledgment

I would like to thank my supervisor, Professor Jun Motoyama, for helping me to complete this research. I would also like to thank him for his support, encouragement, and patience. His approach to scientific research is an inspiration to me and I hope to follow in his creative footsteps.

Furthermore, I would like to thank my mentor, Dr. Koji Oishi, for guiding and participating in my research and making this project possible. I am also grateful for our friendly chats that made my time in this lab thoroughly enjoyable.

I would like to especially thank my committee members, Professor Hiroaki Misono, Professor Takeshi Sakaba, Professor Nobuyuki Nukina, and Professor Naoko Kaneko, for their encouraging words, concern, and feedback.

I would like thank all the members of my lab Kumazaki, Raymond, Akiyama, and Dr. Kidokoro, for their kind support.

Finally, I would like to express my deepest gratitude to my family for their encouragement and understanding, without it, my research would not have been possible.

Table of Contents

LIST OF FIGURES

1. INTRODUCTION

1.1 Overview

Neural progenitor cells (NPCs) are stem cells capable of differentiating into all neuronal and glial cell types in the central nervous system (CNS). Elucidating the mechanisms regulating NPC differentiation is essential for a detailed understanding of brain development. NPCs are not only essential for the development of the nervous system but also play an important role in adult neurogenesis. Intracellular calcium $[Ca^{2+}]_i$ signaling is one of the potential mechanisms regulating NPC development. $[Ca^{2+}]_i$ ions are widely known as second messengers that function intracellularly during cellular responses to extracellular information. Spontaneous fluctuations in $[Ca^{2+}]_i$ have been frequently observed in various processes during embryogenesis and regulate the normal development of NPCs. Although $[Ca^{2+}]_i$ fluctuations play a role in the proliferation and migration of NPCs during cortical development, their role in the differentiation of NPCs into neurons remains largely unknown. Understanding the physiological role of $[Ca^{2+}]_i$ in NPC differentiation will enable the detection of individual NPC status in a living state. Furthermore, it will lead to the developing of new methods to control NPC differentiation. Here, I provide a review of the current literature on the biology of NPCs and the known physiological roles of $[Ca^{2+}]_i$ signaling in neurogenesis.

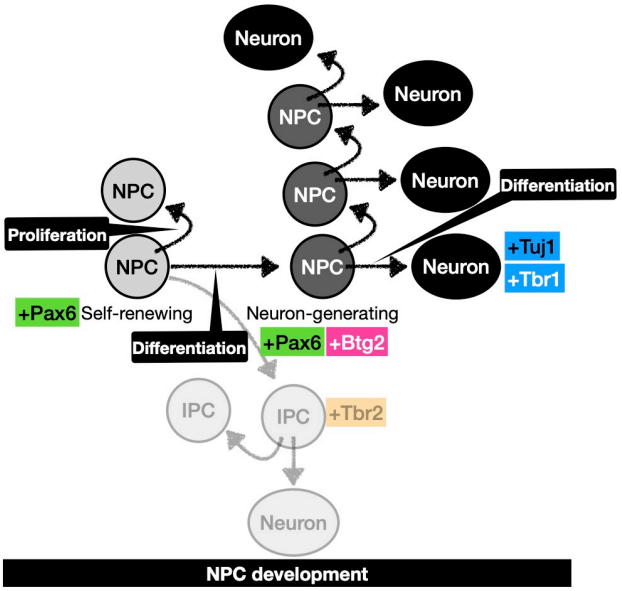

Term	Definition	
Neural progenito cell (NPC)	Undifferentiated cells in the central nervous system can become neurons or glial cells.	Expressing Pax6
Neuron	Cells that can be electrically stimulated and can communicate with other cells through synapses.	Expressing Tuj1 and Tbr1
Self-renewing NPC	NPC that produce other NPC	Expressing Pax6
Neuron-generating NPC	NPC that produce neuron	Expressing Pax6 and Btg2
NPC development	The process produces many neurons and glial cells to create a functioning brain at birth.	
NPC differentiation	The process of morphologically and potentially changes from self-renewing NPCs into neuron-generating NPCs, or intermediate progenitor cells (IPC) or neurons.	
Intermediate Progenitor cell (IPC)	Cells that help NPCs to generate neurons to increases the size and structure of the CNS	Expressing Tbr2

Figure and Table 1.1. Schematic of the NPC development and definitions of terms table.

During the early embryo stage, NPCs proliferate into two NPCs, or these NPCs can self-renew. However, as time progresses, these NPCs differentiate into NPCs that can produce neurons other than themselves. Eventually, the NPCs will differentiate into two neurons. However, understanding the mechanism of how these NPCs can become neurons still needs to be improved.

1.2 Neural development

During mouse embryogenesis from day 7 to day 8.5 after fertilization (E7 to E8.5), ectodermal cells undergo neural induction to differentiate into NPCs and form the neural plate (**Figure 1.2**) (Hitoshi et al., 2004), which undergoes a morphogenetic movement that bends inward, forming a neural tube (**Figure 1.2**). The neural tube is the primordium of the CNS, including the brain and the spinal cord (**Figure 1.2**). The anterior part of the neural tube forms the forebrain vesicle, the primordium of the future cerebrum and basal ganglia.

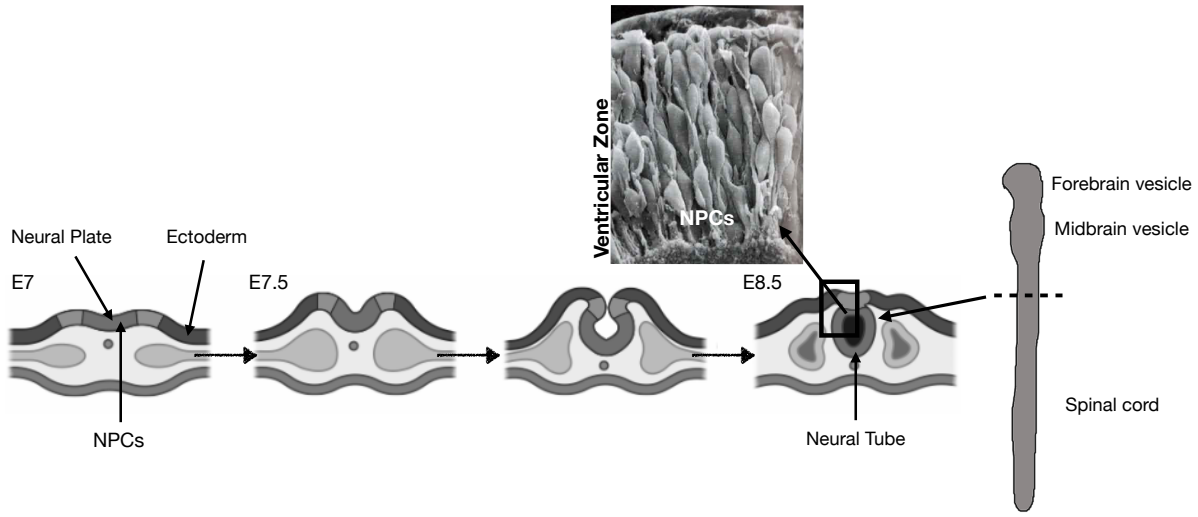

Figure 1.2. Neural tube forming the central nervous system (CNS).

A schematic representation of the neural plate forming the neural tube during embryogenesis. At E7, ectodermal cells differentiate into NPCs, followed by neural plate bending, and the formation of the neural tube around E7.5 to E8.5. The image of NPCs was adapted from the book "Langman's Medical Embryo" (4th edition).

The presumptive cerebral cortex is formed from the dorsal part of the forebrain vesicle, and NPCs localize in the ventricular zone (VZ) facing the lateral ventricle and continue proliferating from E8.5 to E10 (**Figure 1.3**). During this period, NPCs divide into two NPCs, thereby expanding the cell number of NPCs (Cai et al., 2002; Takahashi

et al., 1995). After E11, some self-renewing NPCs begin to differentiate into neurogenic NPCs (**Figure 1.3**), which directly generate immature neurons or differentiate into intermediate progenitor cells (IPCs) that in turn develop into immature neurons (Götz & Huttner, 2005; Noctor et al., 2004). These immature neurons migrate vertically from the VZ toward the surface of the cortex to form the cortical plate (CP). Differentiation into neurogenic or neuron-generating NPCs is a process by which self-renewing NPCs lose their potential "stemness" and produce differentiated cells that reduce their ability to replicate themselves (Fishell & Kriegstein, 2003; Qian et al., 2000). Neuronal differentiation is a complex process by which NPCs acquire electrophysiological characteristics specific to neurons (Luhmann et al., 2016; Murphy et al., 1992). From a morphological point of view, it also increases the size of the cell body, generates more dendrites, and extends its axons further from the cell body to form new connections and integrate networks with other neurons (Horton & Davies, 2020; Kang et al., 2017; Luhmann et al., 2016). However, the mechanisms controlling the differentiation of NPCs remain unclear.

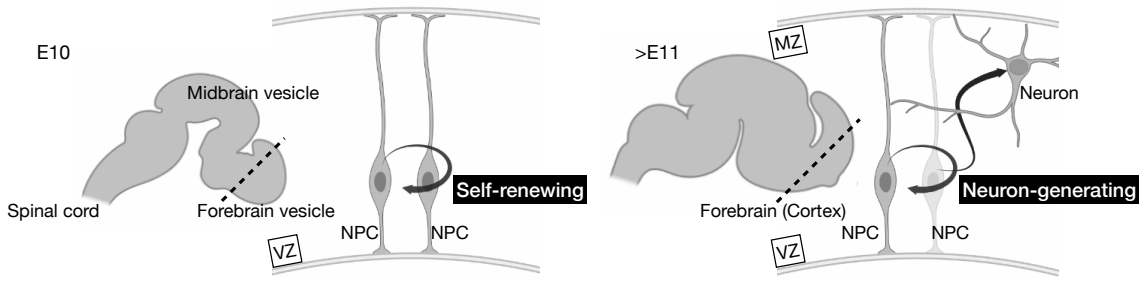

Figure 1.3. Differentiation of self-renewing neural progenitor cells (NPCs).

NPCs are present during the development of the embryonic CNS. In the early stages, self-renewing NPCs proliferate to form two NPCs that increases the pool. Neurogenesis is the generation of neurons by NPCs in the ventricular zone (VZ) during cortical development. At the onset of neurogenesis, self-renewing NPCs differentiate to become neuron-generating NPCs, in which the daughter cell is the neuron.

As described above, neuronal cell generation is through a process by which self-renewing NPCs differentiate into neuron-generating NPCs. These proses regulated by dynamic interactions between intracellular factors, including transcription factors and secreted extracellular signals from neighboring cells (Shi et al., 2008). Pax6 is an essential transcriptional factor for both self-renewing and neuron-generating NPCs in the VZ (**Figure 1.4**). A study using Pax6 gain-of-function transgenic mice and loss-of-function mutants demonstrated that the Pax6 regulation of NPCs was dependent on its levels. Increasing Pax6 levels promoted NPC self-renewal, while reducing Pax6 expression in NPCs decreased the cell cycle regulation, causing premature NPC differentiation into neurons (Sansom et al., 2009). Wnt is one of the secreted proteins regulating the proliferation of self-renewing NPCs in the mouse embryonic brain (Draganova et al., 2015). Mouse embryos with overexpressed Wnt protein in NPCs

resulted in cortical hypertrophy, whereas mouse embryos of loss of function *Wnt* mutants showed a hypotrophic brain (Woodhead et al., 2006). Interestingly, the Wnt/β-catenin pathway is known to activate the Pax6 promoter and induce its transcription, suggesting that Pax6 signaling may have a critical role in self-renewing NPCs, dependent on the Wnt signaling pathway (Gan et al., 2014). However, quantification of cells using fluorescence-activated cell sorting in *Pax6* loss of function condition ($Pax6^{sey/sey}$) revealed that the number of *β*-Tubulin-III-positive neuronal cells was reduced by 50% compared with that in wild-type embryos (Heins et al., 2002), suggesting that Pax6 may also play an essential role in neuron-generating NPCs.

One of the p53-transcriptional targets, Btg2, has previously been identified as an anti-proliferative gene. Pax6 can bind directly to the Btg2 promoter (Sansom et al., 2009), and Btg2 can induce NPCs to exit the proliferative state, switching them to a division mode toward the neurogenic state (**Figure 1.4**). The *Btg2* gene is expressed at low levels from E10.5 to E15.5 while being abundantly expressed in NPCs (Haubensak et al., 2004). Btg2 represses the cyclin D1 promoter, which inhibits the progression of the cell cycle in NPCs, thus promoting NPC differentiation into Tbr1-positive neurons (Englund et al., 2005; Farioli-Vecchioli et al., 2009; Farioli-Vecchioli et al., 2008; Iacopetti et al., 1999). Although several factors that regulate the transition from renewing to neurogenic NPCs have been identified (Solozobova et al., 2012), the molecular mechanisms underlying this regulation remains to be fully understood.

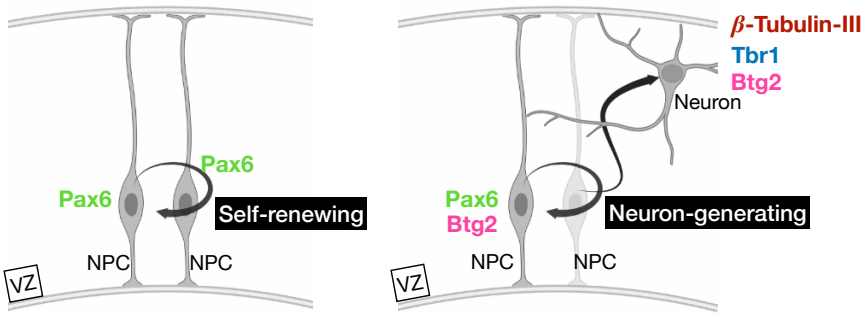

Figure 1.4. Examples of transcription factors regulating the differentiation of self-renewing NPCs.

The transcription factor Pax6 regulates both self-renewing and neuron-generating NPCs in the VZ. The NPCs increase the generation of differentiated cells such as neurons upon expression of the anti-proliferative gene, Btg2. The subsequent differentiation of NPCs to mature neurons is marked by the downregulation of Pax6 and upregulation of Tbr1 or β-Tubulin-III.

1.3 Intracellular calcium ($[Ca^{2+}]_i$) signaling

Calcium (Ca^{2+}) ion is a multifaceted intracellular signaling messenger that regulates several different cellular processes (Berridge et al., 1998); **Table 1.5**). Ca^{2+} ions activate cellular events such as hormonal secretion, cell cycle progression, cell growth, gene expression, pulmonary hypertension, and neurotransmitter secretion (Uhlén & Fritz, 2010). Ca^{2+} signaling plays a significant role in mature cells and tissue function. Moreover, Ca^{2+} signaling is also involved in embryonic events from fertilization to organogenesis and is essential for complex processes such as neuronal, heart, kidney, and muscle cell development (Webb & Miller, 2003).

Cell response	Cell event	Example
Movement	Contraction	Heart beat, leg movement, smooth muscle in the gut
	Chemotaxis	Neutrophils in infection
Secretion	Sebstance released	Hormones and neurotransmitters
	Fluid released	Mucus in the gut
Uptake into the cell	Phagocytosis - particle	Neutrophil engulifing a bacterium
	Endocytosis - membrane	Removal of hormone receptors
	Substrates - fluid	Glucose
	Ions - charged molecule	Ca2+ channels
Electrial excitation	Nerve firing	Action potential
	Muscle firing	Action potential
Fertilisation	Egg	Sperm activation the egg
Cell division	Embryo development	Differentiation
Death	Apoptosis	Lymphocytes after combating an infection

Table 1.5. Example of cellular processes regulated by $[Ca^{2+}]_i$.

Example of cellular events triggered by $[Ca^{2+}]_i$ (adapted from the book "Fundamentals of Intracellular Calcium" by Anthony K. Campbell, 2018).

As a second messenger, $[Ca^{2+}]_i$ is modulated by extracellular chemicals or proteins, and alterations in $[Ca^{2+}]_i$ caused by various extracellular signals result in specific cellular responses (Kapur et al., 2007; Rosenberg & Spitzer, 2011; Schwirtlich et al., 2010; Tsai et al., 2015). Under resting conditions, $[Ca^{2+}]_i$ is maintained at a low level (10–100 nM) compared to extracellular Ca^{2+} (1–10 mM; A.K Campbell, 2018). Stimulus-induced changes in $[Ca^{2+}]_i$ levels are achieved by releasing intracellular Ca^{2+} and/or Ca^{2+} influx from the extracellular space. Ca^{2+} enters the cell from the extracellular space primarily through Ca^{2+} channels (**Figure 1.6)**. For example, voltage-

gated Ca^{2+} channels are Ca^{2+} channels that open when the membrane is depolarized (Catterall, 2011). Then there are Ca^{2+} channels that are activated by protein or hormone binding to cell surface receptors (A.K Campbell, 2018), while the other type of Ca^{2+} channels is activated by intracellular signals such as cyclic adenosine monophosphate (cAMP) or guanosine monophosphate (GMP) (Sperelakis et al., 1994; Vandecasteele et al., 2001). The endoplasmic reticulum (ER) is a well-known source of intracellular Ca^{2+} and Ca^{2+} release from the ER occurs through store-operated calcium entry (SOCE; (Kraft, 2015)). These Ca^{2+} channels are temporarily open, allowing Ca^{2+} influx into the cells, and this increase in intracellular $[Ca^{2+}]_i$ is often referred to as an $[Ca^{2+}]_i$ transient or fluctuation. Interestingly, these $[Ca^{2+}]_i$ fluctuations have been occasionally observed in NPCs during neural tube development (Suzuki et al., 2017).

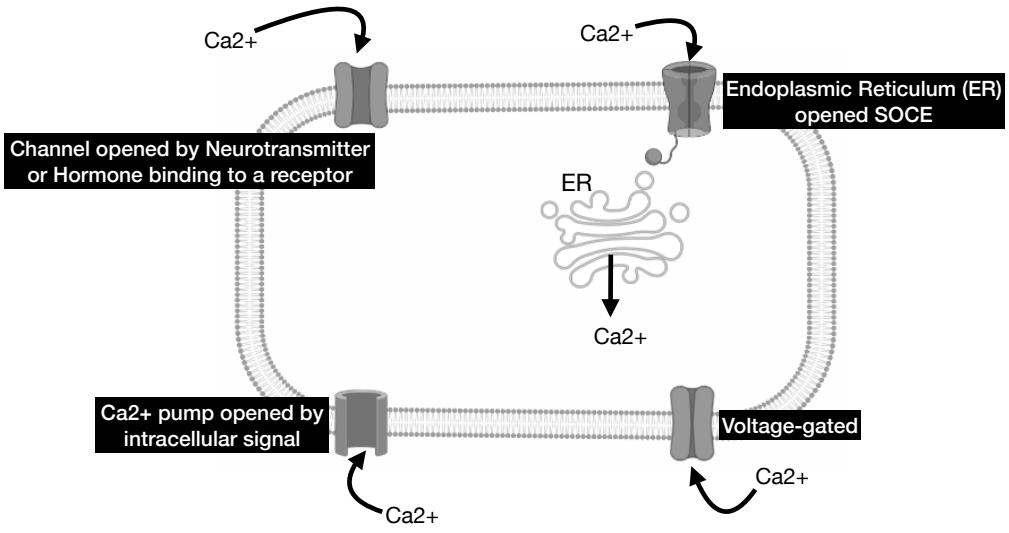

Figure 1.6. Example of Ca^{2+} influx into cells.

Ca^{2+} influx into cells can be mediated by voltage-gated Ca^{2+} channels, extracellular and intracellular hormones, and by ER-regulation of Ca^{2+} storage levels.

1.3.1 $[Ca^{2+}]_i$ fluctuation in neural development

During neural induction, $[Ca^{2+}]_i$ fluctuation has often been observed in the dorsal ectoderm in *Xenopus* embryos (equivalent of E7 in the mouse embryo; (Kawaguchi et al., 2001)). Interestingly, the $[Ca^{2+}]_i$ fluctuation is only observed in the dorsal ectoderm and not in the ventral ectoderm, which develops into surface ectoderm (Leclerc et al., 1997; Leclerc et al., 2000); **Figure 1.7**). This increase in $[Ca^{2+}]_i$ is caused by both Ca^{2+} release from intracellular stores and by Ca^{2+} influx from the extracellular space. Moreover, preloading with the Ca^{2+} chelator BAPTA abolished both $[Ca^{2+}]_i$ fluctuation and neural induction in the dorsal ectoderm of *Xenopus* embryos (Leclerc et al., 2001). Noggin, a BMP signaling antagonist, directly induces both neural differentiation and an increase in $[Ca^{2+}]_i$ fluctuation via an influx through L-type Ca^{2+} channels (Lamb & Harland, 1995; Leclerc et al., 1997). Moreover, exogenous caffeine treatment of the ectoderm also induces NPC differentiation into neurons and increases $[Ca^{2+}]_i$ fluctuation without the effect of Noggin (Moreau et al., 1994). While this study did not investigate whether caffeine treatment could produce normally functioning neurons, the observed correlation between increased $[Ca^{2+}]_i$ fluctuations and neuronal differentiation could be due to neuronal marker expression. Furthermore, previous studies have reported a correlation between Ca^{2+} and cAMP in NPC differentiation (Lepski et al., 2013). Increased cAMP signaling leads to neuronal differentiation by upregulation of voltage-gated Ca^{2+} signaling resulting in increased Ca^{2+} influx, suggesting that Ca^{2+} signaling may be critical for neuronal differentiation (Lepski et al., 2013). Moreover, increased intracellular Ca^{2+} levels also facilitate differentiation in other types of stem

cells (Tonelli et al., 2012). Therefore, changes in intracellular Ca^{2+} levels in NPCs could promote the differentiation of NPCs into mature neurons via a Ca^{2+}-dependent pathway.

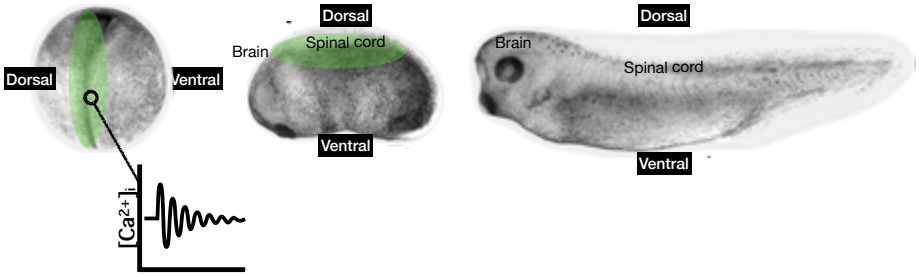

Figure 1.7. $[Ca^{2+}]_i$ fluctuations during neural induction.

During *Xenopus* development, the dorsal ectoderm forms the neural plate which develops into the CNS and the ventral ectoderm forms the epidermis (De Robertis & Kuroda, 2004). $[Ca^{2+}]_i$ fluctuations (green circled area) occur only in the dorsal ectoderm during gastrulation (Leclerc et al., 2000). Figure adapted from Xenbase (https://www.xenbase.org/entry/anatomy/intro.do).

In the mouse embryo, neurogenesis occurs between E10 and E17 (Eckenhoff & Rakic, 1988). While some NPCs begin to differentiate into immature neurons at E10–11, most NPCs in these stages are still self-renewing. During E14–16, most NPCs are in the neurogenic state, with several NPCs becoming neuron-generating NPCs (Haubensak et al., 2004). The cells showing $[Ca^{2+}]_i$ fluctuations in the VZ were identified to be developing cortical NPCs during E14–16 (Owens & Kriegstein, 1998; Weissman et al., 2004). Moreover, $[Ca^{2+}]_i$ fluctuations have been observed not only in NPCs but also in various stem cell lines, including mesenchymal stem cells (Kawano et al., 2002), suggesting that $[Ca^{2+}]_i$ fluctuations may play an essential role in stem cell development.

Kriegstein's group reported on spontaneous $[Ca^{2+}]_i$ signaling in the embryonic rat VZ cortex (LoTurco et al., 1995) and described a stage-dependent pattern of $[Ca^{2+}]_i$ fluctuation in the rat VZ cortex, with $[Ca^{2+}]_i$ fluctuating at a higher frequency and traveling over a longer distance at E16–17 than that at E12–13 in rat NPCs (Owens & Kriegstein, 1998; Rash et al., 2016; Weissman et al., 2004). The $[Ca^{2+}]_i$ fluctuation at E16–17 appeared to be mediated by Ca^{2+} release from intracellular stores and regulated by extracellular ATP signaling (Owens & Kriegstein, 1998; Weissman et al., 2004). Furthermore, disruption of $[Ca^{2+}]_i$ fluctuations by ATP receptor antagonists resulted in decreased cell proliferation in the VZ (Weissman et al., 2004), indicating that Ca^{2+} signaling is involved in NPC proliferation. Other investigators have also reported that inhibition of extracellular ATP signals by ATP receptor antagonists or purinergic P2Y1 receptor antagonists effectively blocked $[Ca^{2+}]_i$ fluctuations, resulting in impaired cell proliferation in the VZ, and simultaneously blocked the migration of IPCs (Liu et al., 2008). Inhibitors of gap junctions also block $[Ca^{2+}]_i$ fluctuations in the VZ, suggesting that synchronous $[Ca^{2+}]_i$ fluctuations are radially propagated through connexin hemichannels (Malmersjö et al., 2013; Weissman et al., 2004). Disruption of $[Ca^{2+}]_i$ fluctuations via inhibition of gap junctions also leads to decreased cell proliferation in the VZ (Malmersjö et al., 2013; Weissman et al., 2004). Synchronous Ca^{2+} waves propagate through the gap junctions among the daughter cells of a single NPC, and the $[Ca^{2+}]_i$ wave patterns may act as a pacemaker of NPC proliferation and migration. However, previous studies have focused on the role of $[Ca^{2+}]_i$ fluctuations in NPC cell proliferation and IPC migration or the migration of immature neurons during cortical development during late gestational stages (such as E15, 17, and 19). Thus, little is

known about the role of $[Ca^{2+}]_i$ fluctuations in NPCs during early developmental stages, especially during their differentiation from NPCs to neurons.

1.4 AIMS

The mechanisms underlying the maintenance of NPCs in the VZ in a self-renewing state and the neuronal differentiation of their daughter cells remain unknown. In this study, we focused on the previously uncharacterized role of $[Ca^{2+}]_i$ fluctuations during the differentiation of NPCs into neurons. Identifying a correlation between $[Ca^{2+}]_i$ fluctuation patterns and neural differentiation would enable deciphering the developmental state of each NPC under live conditions. Thus, this thesis aimed to investigate whether $[Ca^{2+}]_i$ fluctuations in NPCs are involved in regulating their differentiation. The specific aims were:

A. We investigated whether NPCs from early to late developmental stages (at E11, 12, 14, and 16) in the VZ cortex exhibited distinct $[Ca^{2+}]_i$ fluctuation patterns. We then classified the pattern of the observed $[Ca^{2+}]_i$ fluctuations in undifferentiated NPCs, neuron-generating NPCs, and immature neurons.

B. We examined the role of the $[Ca^{2+}]_i$ fluctuations in NPC proliferation and differentiation using two approaches: first, by treating *in vitro* neurosphere cultures with an inhibitor against a specific Ca^{2+} channel and second, by

knocking down the expression of the specific Ca^{2+} channel during NPC development *in vivo*.

2. MATERIALS AND METHODS

2.1 Tissue preparation for immunohistochemistry of BrdU and EdU

We investigated the proliferation rate of VZ NPCs by injecting pregnant mice at different developmental stages (E11, E13, and E15) with 50 µg/g body weight 5-Bromo-2'-deoxyuridine (BrdU) for 24 hours. These times were selected to label the cell cycle (S, G2, M, and G1) with a combined injection of 5-ethynyl-2'-deoxyuridine (EdU) 1.5 h before the end of 24 hours BrdU treatment. The Click-iTTM EdU Alexa FluorTM 488 Imaging Kit (Invitrogen, Thermo Fisher Scientific) was used to label cells primarily in the S phase to identify the cells that return to the cell cycle as renewable cells. For detecting cells that exited the cell cycle, we combined BrdU analysis with Ki67. After 24 h, embryos were exposed by cesarean section, decapitated, and the heads were fixed overnight in 4% paraformaldehyde at 4°C. After washing with phosphate-buffered saline (PBS) (137 mM NaCl, 2.7 mM KCL, 10 mM Na_2HPO_4, and 1.8 mM KH_2PO_4, pH 7.4), 10 µm paraffin coronal sections were made. The sections were rinsed in PBS, permeabilized, and blocked with 0.5% Triton X-100 for 20 min at room temperature (RT). Cortical tissues were then incubated overnight at 4°C with 1× iTTM reaction buffer $CuSO_4$ and Alexa Fluor Azide 488 and anti-BrdU mouse monoclonal primary antibody (1:100 dilution) in PBS containing 2% Gelatin and bovine serum albumin (BSA). The tissues were washed and incubated for 1 hour at RT with an anti-mouse secondary antibody (1:200 dilution) in PBS with 2% Gelatin and BSA. After washing, the tissue was visualized using laser confocal microscopy.

2.2 Tissue preparation for calcium imaging

Calcium imaging was performed on acute neocortex slices from mouse embryos at E12, E14, and E16. Pregnant mice (ICR, Shimizu laboratory supplies, Japan) were anesthetized with an intraperitoneal injection of avertin (0.25 mg/g body weight), and the embryos were isolated by cesarean section. The embryos were decapitated, and the heads were immediately placed in ice-cold PBS. The whole brains isolated from embryos were embedded in 3–4% low-melting agarose at 30–35°C (Lonza, Switzerland), hardened on ice, and sliced into coronal sections (500 μm thickness) with a vibratome (D.S.K, Japan). The acute slices were collected in an ice-cold medium (DMEM/Ham's F-12, Nacalai, Japan) oxygenated with 95% O_2/5% CO_2. For calcium imaging of cells derived from the embryonic cortex at E11, 12, 14, and 16, the isolated neocortex explants were dissociated by repeated gentle pipetting in the ice-cold medium. The cells were then incubated in a poly-L-lysine-coated glass base dish (AGC techno glass co., ltd. Japan) at a density of 4–5×10^6 cells/ml for 1 h at 37℃ in a CO2 incubator (Sanyo, Japan) to allow the cells to attach to the glass base.

2.3 Calcium imaging

We used the calcium indicator dye Fluo-4 acetoxymethyl (AM) (Dojindo, Japan, (Kraft et al., 2017; Yuryev et al., 2018; Yuryev et al., 2015)) to visualize the temporal changes in $[Ca^{2+}]_I$ levels. Brain slices were incubated in the oxygenated medium containing 1× N-2 supplement (Thermo Fisher Scientific, USA) and 1 μM Fluo-4 AM for 30 min at 37°C under dark conditions. The slices and cells were then washed in oxygenated

artificial cerebrospinal fluid (ACSF) (138.6 mM NaCl, 3.35 mM KCl, 0.6 mM $NaH_2PO_4.2H_2O$, 2.1 mM $NaHCO_3$, 9.9 mM Glucose, 1 mM $MgCl_2$, and 2 mM $CaCl_2$, pH 7.4) three times for 5 min each at 37°C before imaging. The brain slices were then placed in an imaging chamber containing oxygenated ACSF on the stage of a microscope (40×; NA, 0.75 objectives, BX51, Olympus, Japan). The attached cells were also incubated in the culture medium containing 1 μM Fluo-4 AM for 30 min at 37°C in the CO2 incubator (Sanyo, Japan). The cells in the glass base dish were also placed on the stage of the inverted microscope (40×; NA, 0.75 objectives, BX51, Olympus, Japan). To record the temporal changes in the Fluo-4 AM signal, illumination was provided by the laser scanning confocal attachment (FV300 for slices, FV1000 for cells, Olympus, Japan). The excitation and emission wavelengths for Fluo-4 AM were 488 and 515 nm, respectively. We used an argon laser as the laser source of 488 nm visible light. The laser intensity was 10%, and the photomultiplier tube was loaded with a voltage of 670 V in all recording experiments. Generally, one image was acquired every 8.3 s/frame. All imaging experiments were performed at 21–25°C (Chemin et al., 2002; Owens & Kriegstein, 1998; Rodríguez-Gómez et al., 2012; Weissman et al., 2004). Image processing and quantification of fluorescence signal in each frame were performed using ImageJ (National Institutes of Health, USA). We used regions of interest (ROIs) in a round shape covering the cell body exhibiting a Fluo-4 AM signal in each frame to quantify the fluorescence signal of each cell at each time point (F_t). To describe the temporal change patterns in Fluo-4 AM signal in the brain slices, we used F_t indicated as "Brightness (Fluo-4 AM)." This is raw data without any calibration. For calcium imaging of cells derived from the embryonic cortex, we calibrated the value of

the Fluo-4 AM signal for each cell (F_t) using the value of the Fluo-4 AM signal for each cell after treatment with ionomycin (F_{max}). We quantified the Fluo-4 AM signal for each ROI at each time point (F_t) among cells at different developmental stages, and then the Ft of each cell was divided by Fmax. Fmax represents the fluorescence intensity of Fluo-4 AM after treatment with ionomycin. We recorded the value of F_{max} after recording F_t in all experiments. Since no significant difference was observed between E11 and E16 in the F_{max} mean among Pax6-positive and Tuj-1-positive cells (**Figure 2.1F, G**), we used F_t/F_{max} to compare the pattern and average amplitude of calcium fluctuations among self-renewing NPCs, neuron-generating NPCs, and immature neurons. To examine the pattern of spontaneous $[Ca^{2+}]_i$ fluctuations, we classified the recorded cells into cells displaying intermittent $[Ca^{2+}]_i$ transients (**Figure 2.2A, I, J**) and cells without the $[Ca^{2+}]_i$ transients (**Figure 2.2A, G, H**). The intermittent $[Ca^{2+}]_i$ transient was defined as the change in the F_t value reaching more than 50% of the mean of the whole F_t value in one recording and go above the baseline. The duration between the start and convergence of the change was less than 166 seconds or 20 frames during one recording (Ferrari et al., 1996). The amplitude of the intermittent $[Ca^{2+}]_i$ transient was calculated using the following formula: $(F_t-F_0)/ F_0$ (**Figure 2.2G-J**). F_0 was defined as the minimum value of fluorescence during the observation (**Figure 2.2G-J**). The mechanisms of spontaneous $[Ca^{2+}]_i$ fluctuations were examined using acute brain slices and cells attached on the glass base, treated with Ca^{2+}-free ACSF containing 5 mM EGTA (Sigma-Aldrich, USA), 5 μM ionomycin (Fujifilm, Japan), and calcium channel blockers: 20 μM Nifedipine, 10 μM Mibefradil, and 2.5 μM NNC55-0396 (Cayman Chemical, USA).

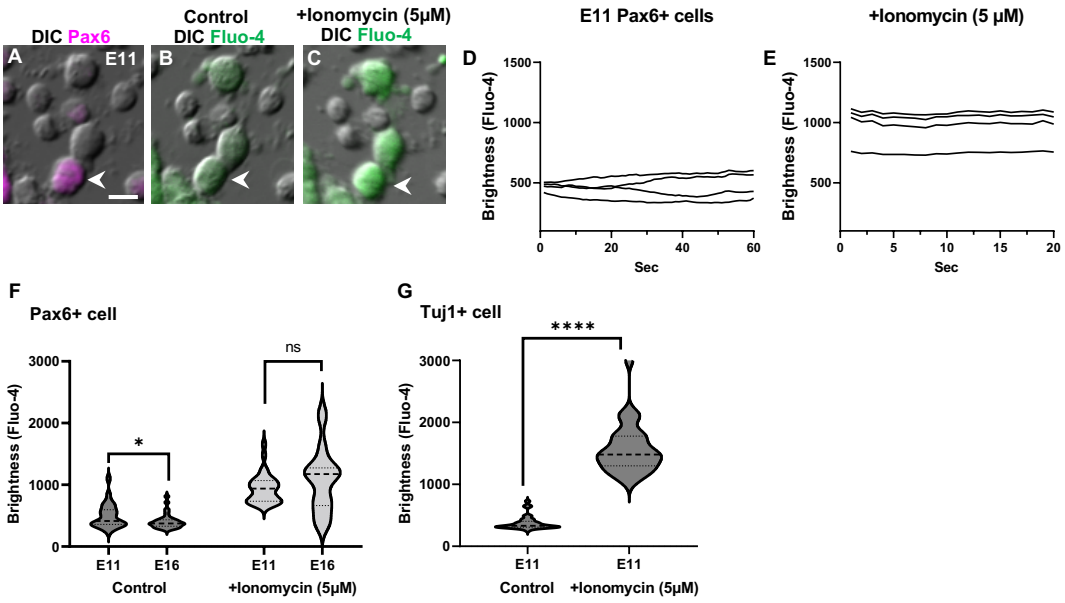

Figure 2.1. Effect of ionomycin on the Fluo-4 AM signal in Pax6 and Tuj1-expressing cells.

(A–C) To compare the Fluo-4 AM signal between control and ionomycin (5 μM)-treated Pax6-positive cells (A), calcium imaging was performed in medium containing 5 μM of ionomycin (C) after recording in the control conditions (B). Scale bar in (A) is 10 μm for (A–C). (D, E) Example of patterns of temporal change in Fluo-4 AM signal in Pax6-positive cells at E11 in the control (D) and with 5 μM of ionomycin (E). Note the significant increase in the brightness (Fluo-4 AM) when the culture condition was changed from control to that with 5 μM ionomycin (E). (F) Furthermore, there was no significant difference in the average brightness (Fluo-4 AM) between E11 and E16 after treatment with 5 μM ionomycin, suggesting that Fluo-4 AM uptake in cells expressing Pax6 was not significantly different between E11 and E16 (n=33 in ionomycin at E11, n=21 at E16). (G) To find F_{max} value in Tuj1-positive cells, calcium imaging of Tuj1-positive cells at E11 was performed in medium containing 5 μM ionomycin. Note the significant increase in the brightness (Fluo-4 AM) when the culture condition was changed from control to that with 5 μM ionomycin (G).

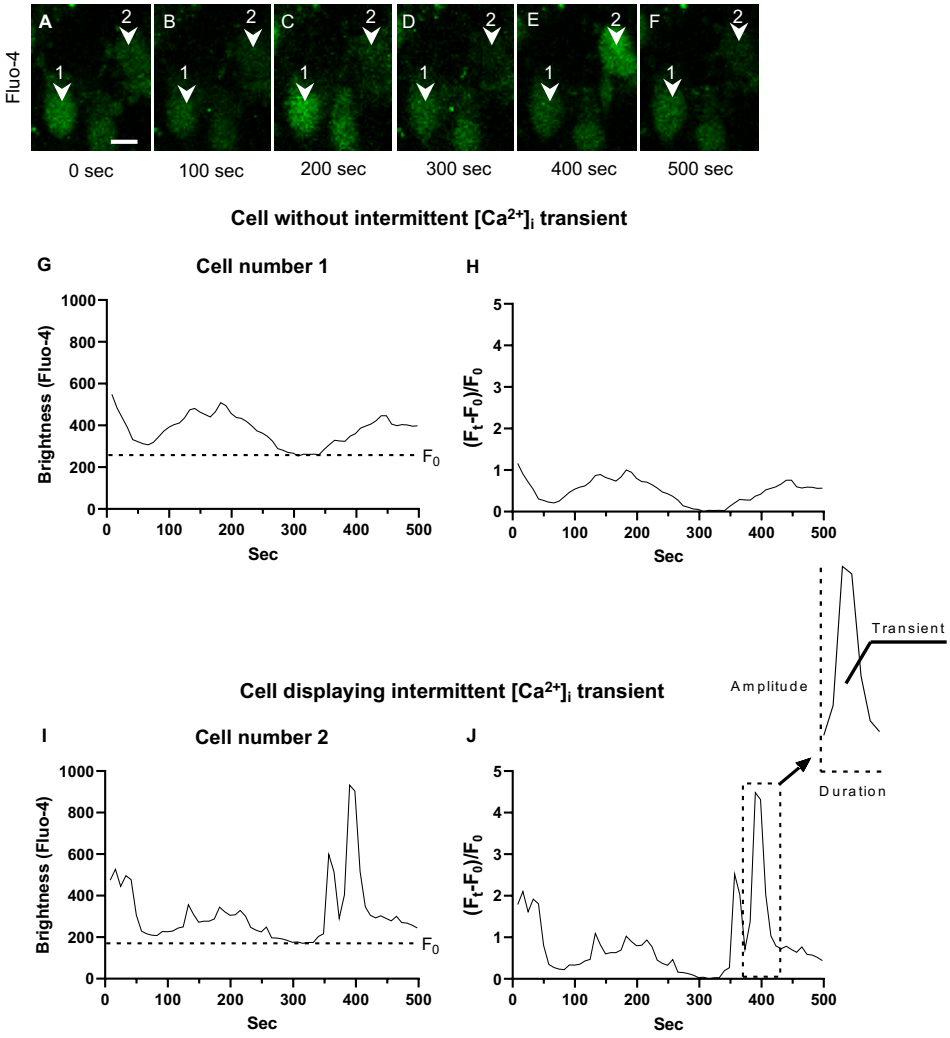

Figure 2.2. Analysis of intermittent $[Ca^{2+}]_i$ transients in $[Ca^{2+}]_i$ fluctuations.

The intermittent $[Ca^{2+}]_i$ transient was defined as the change in the fluorescence signal reaching to more than 50% of the mean fluorescence signal of Fluo-4 AM per imaging (8.3 min) and the duration between the start and convergence of the change was less than 166 seconds. (A–F) The Fluo-4 AM fluorescence signal in VZ cells was recorded as a temporal change in $[Ca^{2+}]_i$. Scale bar in (A) is 10 μm for (A–F). (G, H) Typical example of temporal changes in Fluo-4 AM fluorescence intensity without intermittent $[Ca^{2+}]_i$ transient as shown by cell number 1 (indicated by arrowheads 1 in A–F). Temporal changes in Fluo-4 AM signal did not meet the criteria for intermittent $[Ca^{2+}]_i$ transient (H). (I–J) An example of temporal changes in Fluo-4 AM fluorescence intensity with intermittent $[Ca^{2+}]_i$ transient as shown by cell number 2 (indicated by arrowheads 2 in A-F). The amplitude and duration of intermittent $[Ca^{2+}]_i$ transient was calculated using the formula: $(F_t-F_0)/ F_0$. F_0 was defined as the minimum fluorescence signal intensity detected during observation (J).

2.4 Evaluation of viability of acute slices and cells isolated from embryonic cortex

We evaluated the viability of the acute brain slices during $[Ca^{2+}]_i$ Fluo-4 AM signal recording by monitoring mitochondrial membrane potential in the VZ cells using Mitotracker (CMXRos; Invitrogen, USA). Acute embryonic brain slices were incubated with an oxygenated culture medium containing both 1 μM Fluo-4 AM and 1 μM Mitotracker for 30 min at 37°C under dark conditions. The Mitotracker signal was analyzed using the shape of each mitochondria and measuring Mitotracker fluorescence within the ROI indicated by the square shape within the 0.004 mm^2 area of the VZ region. Fluorescence in the ROI was quantified as Mitotracker signal intensity, and its temporal fluctuation was examined without calibration. To check the viability of cells isolated from the embryonic cortex, we detected dead cells in the glass base dishes after incubating cells in a culture medium containing 2 μg/ml Propidium Iodide (PI; Nacalai, Japan) for 30 min in a CO^2 incubator.

2. 5 Identification of cell types after imaging

After calcium imaging of cells isolated from the embryonic cortex, the cells were processed for immunochemistry for cell type identification. Maps were created from artificial landmarks to identify the location of all cells in the frame. This map allowed the calcium imaging results to be superimposed on the results of subsequent immunohistochemical analyses. After live calcium imaging, the cells were fixed in 4% paraformaldehyde for 20 min at RT. The cells were washed in PBS and then permeabilized and blocked with 0.5% Triton X-100 for 20 min at RT. The cells were

then incubated for 16 h at 4°C with antibodies against Pax6, Btg2 (Funakoshi, Japan), Tbr1, and Tuj1 (Biolegend, USA) proteins at 1:200–500 dilutions in PBS containing 2% gelatin and 1 mg/ml BSA (Sigma-Aldrich, USA). Next, the cells were washed and then incubated for 1 h at RT with anti-mouse/rabbit IgG antibodies (1:400–500 dilution) (Invitrogen, USA) in PBS with 2% gelatin and 1 mg/ml BSA. After washing, the samples were observed using a confocal microscope. The images obtained by immunohistochemistry were then combined with those of calcium imaging and differential interference contrast (DIC) images to identify the cell types showing calcium fluctuations.

2. 6 Neurosphere culture

Neurosphere cultures were established as previously reported (Chiasson et al., 1999; Vescovi & Snyder, 1999; Weiss et al., 1996). Cells were isolated from the embryonic cortex at E12 by dissociating the neocortex explants using a combination of papain (Nacalai, Japan), DNase I (Roche Diagnostics, USA), trypsin inhibitor (Sigma-Aldrich, USA), and repeated pipetting, and then cultured in uncoated 96-well (200 μL/well) plates (Thermo Fisher Scientific, USA) at a cell density of 2×10^5 cells/ml in culture medium (DMEM/Ham's F-12, Nacalai, Japan) containing 1× B-27 supplement (Thermo Fisher Scientific, USA), 10 ng/ml FGF2 (Sigma-Aldrich, USA), and 10 ng/ml EGF (Sigma-Aldrich, USA). After five days of incubation, the number of neurospheres with a diameter of >100 μm or <100 μm were counted. Secondary neurospheres were collected by dissociating the primary spheres described above and cultured in the same conditions as the primary spheres. After five days of culture, the number of

neurospheres was counted as described above. To examine the effect of T-type calcium channel inhibition on sphere formation, we used medium containing 1, 2.5, and 5 μM NNC55-0396 (Cayman Chemical Company, USA).

2.7 Knockdown of Cav3.1 and Cav3.2 using in utero electroporation

The pSuper-puro plasmid (Oligoengine, USA) containing the H1 RNA promoter for the expression of short hairpin RNA (shRNA) was used to construct the shRNA-encoding plasmid. The inserted sequence was 5′-GGGCTGCTCTTTACTTCATCGcgaaCGATGAAGTAAAGAGCAGCCC-3′ (the lowercase letters indicate the loop sequence) for Cav3.1 (Cacna1g) shRNA and 5′-GATCCCGCTTGGGAACGTGCTTCTTCTcgaaAGAAGAAGCACGTTCCCAAGC TTTTTTC-3′ for Cav3.2 (Cacna1h) shRNA. In-utero electroporation was carried out as described previously (Tabata & Nakajima, 2001). Briefly, shRNA expression vectors (4 mg/ml) were injected together with the pCAGGS vector carrying the enhanced GFP cDNA (1 mg/ml) into the lateral ventricle of the intrauterine E14.5 embryos, and electric pulses (33 V, 50 ms, 4 times) were then applied using an electroporator with a forceps-type electrode. After 24 h, brains were isolated, fixed for 1 h in 4% paraformaldehyde at 4°C, and incubated for 16 h at 4°C with 20% sucrose in PBS (wt/vol), embedded in OCT compound (Sakura Finetek, Japan), and sectioned using a cryostat to obtain coronal sections (14 μm thickness). The sections were subjected to immunohistochemical analysis.

2. 8 Immunohistochemistry

To examine the effect of T-type calcium channel knockdown on neural differentiation, frozen embryonic brain sections (14 μm thickness) were incubated for 16–20 h at 4°C with antibodies against Pax6 (Biolegend, USA) and Tbr1 (Cell Signaling, USA) at 1:200–500 dilutions in PBS containing 2% gelatin and BSA. The sections were washed, incubated for 1 h at RT with anti-mouse/rabbit secondary antibodies labeled with a fluorescent dye (Invitrogen, USA) diluted at 1:400–500 in PBS containing 2% gelatin and 1 mg/ml BSA and washed again in PBS. Finally, the antibody signal was visualized using laser confocal microscopy. We also performed whole-mount immunostaining to detect Tbr1-positive immature neurons in neurospheres. Cultured neurospheres were fixed in the culture plate for 20 min in 4% paraformaldehyde at 4°C and then washed in PBS. The spheres were permeabilized with 0.5% Triton X-100 and then blocked to avoid nonspecific antibody binding with PBS containing 2% gelatin and BSA. The neurospheres were then incubated with antibodies against Tbr1 at 1:500 dilution in PBS containing 2% gelatin and BSA for 16 h at 4°C. The spheres were washed and incubated for 1 h at RT with an anti-mouse secondary antibody labeled with a fluorescent dye diluted at 1:400–500 in PBS containing 2% gelatin and 1 mg/ml BSA and washed again in PBS. Finally, the distribution of Tbr1-positive cells in the spheres was visualized using laser confocal microscopy (FV300, Olympus, Japan).

2. 9 EdU labeling

To label the cells in the S-phase, pregnant mice were injected with 2.5 mg/ml of EdU (Thermo Fisher Scientific, USA) for 1.5 h. After 1.5 h, the embryos at E12, E14, and E16 were exposed by cesarean section, fixed in 4% paraformaldehyde (Nacalai, Japan) for 16 h at 4°C, and then washed in PBS. Paraffin-embedded coronal sections were prepared (10 μm thickness). The sections were rinsed in PBS, permeabilized, and then blocked with 0.5% Triton X-100 for 20 min at room temperature (RT; 21–25°C). EdU was detected using Click-iT™ EdU Cell Proliferation Kit for Imaging (Thermo Fisher Scientific, USA) following the manufacturer's protocol.

2. 10 Data analysis

Data sets were analyzed using GraphPad Prism and Microsoft Excel spreadsheets. Statistical analysis was performed with a two-tailed Student's t-test, and *p*-values of <0.05 were considered statistically significant.

3. RESULTS

Neural stem cells undergo proliferative and differentiation phases depending on gestational age, transforming into different neuronal types. In the CNS, Ca^{2+} signaling is a critical second messenger for various neural functions, including axon guidance, excitatory neuronal transmission, and neural circuit formation. This study demonstrates the role of Ca^{2+} signaling in NPC differentiation.

3.1 Developmental change in the proliferation ratio of VZ NPCs

The balance between the ratio of NPC cell proliferation and differentiation during cortical development varies among the developmental stages. Before investigating whether Ca^{2+} signaling in NPCs is directly related to these processes, we examined the changes in this balance in NPCs by analyzing the proliferation ratio of NPCs in the VZ. BrdU and EdU were used at E12, E14, and E16 to estimate the percentage of cells that continued to proliferate for 24 hours (**Figure 3.1)**. The proliferation rate was calculated as the number of BrdU and EdU double-positive cells (cell cycle re-entering cells) divided by the total number of BrdU-positive cells in the VZ. We observed that the proliferation rate of cells inside the VZ gradually decreases over the course of development. (E12: 53.11 ± 4.0%; E14: 30.08 ± 2.176%; E16: 20.27 ± 1.502%; **Figure 3.2A–D**), indicating that NPCs undergo changes during embryonic progression. The decrease in the proliferative capacity of NPCs is thought to be due to NPC differentiation into neurons after cell cycle completion (Buttitta & Edgar, 2007).

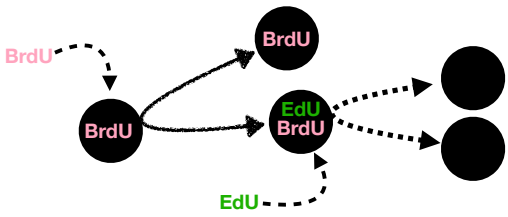

Figure 3.1. Detection of continuing proliferative cells.

Typical proliferating mammalian stem cells have an average cell cycle of 24 h (Masnadi-Shirazi et al., 2019). To identify proliferative NPCs, we introduced BrdU, which is incorporated into dividing cells and is inherited by daughter cells. We used EdU after 24 h to identify the cells that continued to proliferate; EdU is also incorporated into dividing cells. Thus, BrdU/EdU double-positive cells will indicate continuously proliferating cells.

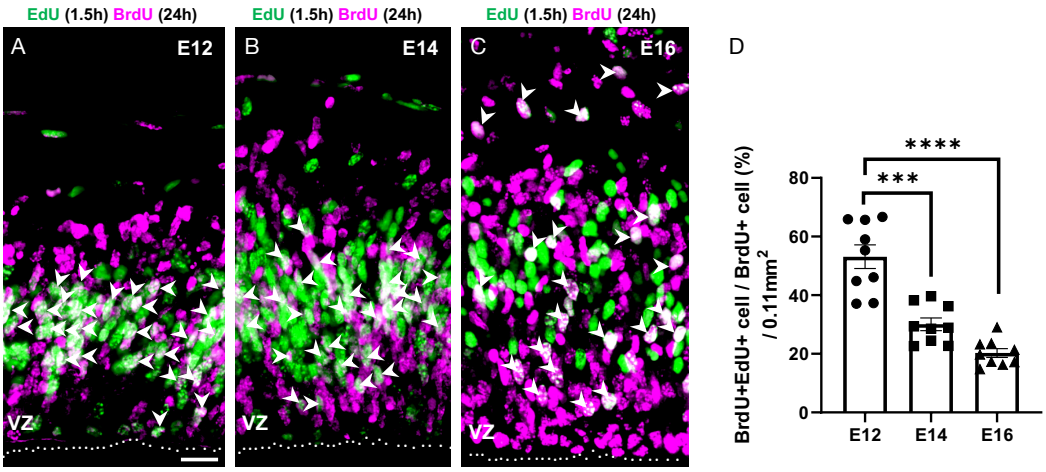

Figure 3.2. Proliferation of VZ cells during development.

(A–C) Detection of continuously proliferative cells in the developing cortex at E12 (A), E14 (B), and E16 (C). Arrowheads indicate BrdU/EdU double-positive cells (A, B, C). Scale bar is 30 µm for (A–C). The ratio of BrdU/EdU double-positive cells to total number of BrdU-positive cells reduced from E12 (n=9) to E14 (***p=0.0001; n=9), and E16 (****p=<0.0001; n=9). Values are mean ± SEM.

3.2 Pattern of $[Ca^{2+}]_i$ fluctuations in the VZ during development.

We investigated the role of $[Ca^{2+}]_i$ fluctuations in NPC development by observing $[Ca^{2+}]_i$ fluctuations in the cortical VZ region in acute brain slices prepared from mouse embryos at E12, E14, and E16. The temporal changes in $[Ca^{2+}]_i$ fluctuations detected by the Fluo-4 AM signal in individual cells were recorded for 8.3 min using a confocal microscope. The VZ region was defined as the area between the position of S-phase cells detected by EdU and the ventricular surface (**Figure 3.3A, D, G**). In the VZ, several cells showed fluctuations in the Fluo-4 AM signal at all three stages (**Figure 3.3B, C, E, F, H, I**). The number of cells with fluctuations in Fluo-4 AM signal in the VZ (0.013 mm^2 as unit area) was the highest at E14, followed by that at E12, and was the lowest at E16 (**Figure 3.3J**).

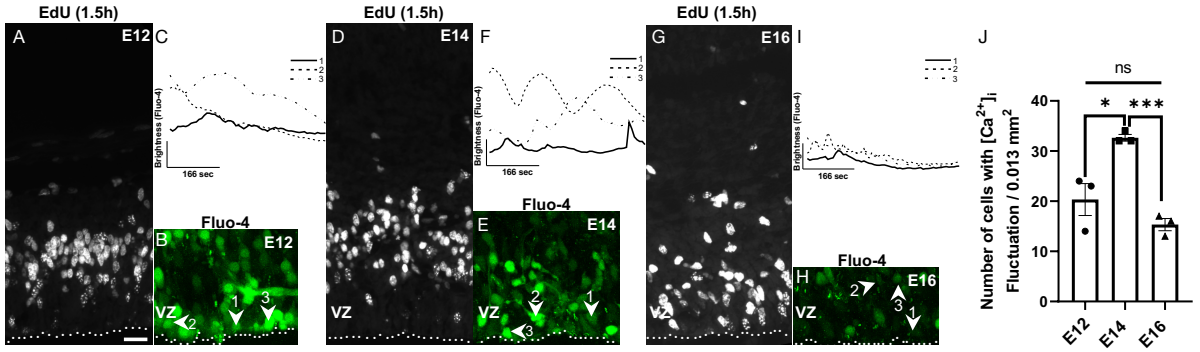

Figure 3.3 $[Ca^{2+}]_i$ fluctuations in the VZ at E12, E14, and E16.

(A, D, G) Detection of proliferative cells in the developing cortex at E12 (A), E14 (D), and E16 (G). The VZ region was determined using EdU labeling for 1.5 h. (B, E, H) The Fluo-4 AM fluorescence signal was recorded for 8.3 min as temporal $[Ca^{2+}]_i$ changes in the VZ, as defined by the distribution of EdU+ cells at E12 (A, B), E14 (D, E), and E16 (G, H). Scale bar in (A) is 20 μm for (A, B, D, E, G, H). Dotted lines in (A, B, D, E, G, H) indicate the ventricular surface. The imaging area was 0.019 mm^2 at E12 (B), 0.022 mm^2 at E14 (E), and 0.013 mm^2 at E16 (H). (C, F, I) Temporal changes in Fluo-4 AM fluorescence intensity are shown by the numbered cells (indicated by arrowheads 1–3 in B, E, H). The brightness (Fluo-4 AM) is the absolute value under the same detection condition for all stages (C, F, I). (J) The number of cells with fluctuations in Fluo-4 AM signal at E14 was significantly higher than that at E12 (*p=0.0192) and E16 (***p=0.0002). There was no significant difference in the number of cells exhibiting fluctuations in Fluo-4 AM signal between E12 and E16 (J). Values are mean ± SEM.

Among the patterns of Fluo-4 AM signal fluctuation, we found cells in which the Fluo-4 AM fluorescence intensity changed rapidly over a short period (**Figure 2.2**). This change in Fluo-4 AM fluorescence intensity may indicate intermittent $[Ca^{2+}]_i$ transients. Cells showing fluctuations in Fluo-4 AM signal were classified into two groups according to the presence or absence of this intermittent $[Ca^{2+}]_i$ transient (**Figure 2.2**). Among the cells displaying Fluo-4 AM signal fluctuations in the VZ at E12, 56.3% of them did not exhibit intermittent $[Ca^{2+}]_i$ transients (**Figure 3.4A, C**), whereas 43.6%

of them exhibited the $[Ca^{2+}]_i$ transients (**Figure 3.4B, C**). In contrast, at E14, 64.6% of VZ cells showed intermittent $[Ca^{2+}]_i$ transients, while 35.3% did not (**Figure 3.4C**). At E16, more than 73.6% of the cells displayed $[Ca^{2+}]_i$ transients, whereas 26.3% of cells did not (**Figure 3.4C**). Taken together, the number of cells exhibiting Fluo-4 AM signal fluctuations without intermittent $[Ca^{2+}]_i$ transients per unit area was highest at E12 than at other stages, whereas the number of cells with intermittent $[Ca^{2+}]_i$ transients was highest at E14 (**Figure 3.3J, Figure 3.4C)**.

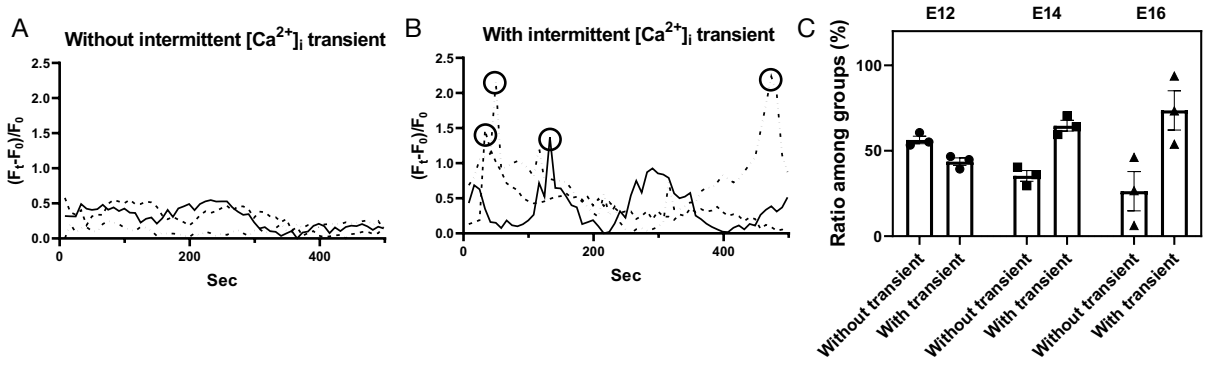

Figure 3.4 Classification patterns of temporal changes in Fluo-4 AM signal.

(A, B) The Fluo-4 AM temporal change patterns were classified into two groups based on without (A) or with intermittent $[Ca^{2+}]_i$ transients (B). The peak of the intermittent $[Ca^{2+}]_i$ transient was indicated by a circle in (B). (C) shows the ratio of the two groups at each stage. No significant difference was observed in the ratio between cells without and with intermittent $[Ca^{2+}]_i$ transients at E12 (M). The number of cells with $[Ca^{2+}]_i$ transients at E14 and E16 was higher than that without intermittent $[Ca^{2+}]_i$ transients (C). Values are mean ± SEM.

We also examined differences in the average Fluo-4 AM signal intensity among the developmental stages. The average Fluo-4 AM signal at E12 was 572.2 ± 45.05, which was significantly higher than that at E14 (406.1 ± 20.56) and E16 (205.2 ± 9.03) (**Figure 3.5A**). The frequency of the intermittent $[Ca^{2+}]_i$ transients was lower at E12

than that at E14 and E16 (**Figure 3.5B**). The duration of the observed transient at E12 was longer than that at E14 and E16 (**Figure 3.5C**). The mean amplitude of the intermittent $[Ca^{2+}]_i$ transient was higher at E12 than at the other stages (**Figure 3.5D**). Thus, these observations suggested that the cells in VZ tend to generate more intermittent $[Ca^{2+}]_i$ transients with short duration and lower amplitude according to their developmental progress.

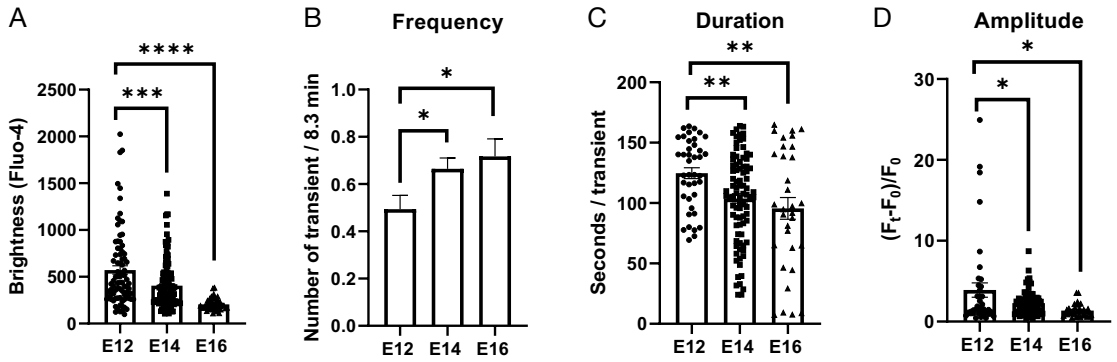

Figure 3.5 Fluo-4 AM intensity, frequency, duration, and amplitude transient in $[Ca^{2+}]_i$ fluctuations.

(A) Average Fluo-4 AM signal intensity per cell was compared among E12, E14, and E16 stages. The average Fluo-4 AM signal per cell at E12 (n= 83) was significantly higher than that at E14 (***p=0.0002, n=143), and E16 (****p<0.0001, n=46). (B) The mean number of intermittent $[Ca^{2+}]_i$ transients per observation. The number of each intermittent $[Ca^{2+}]_i$ transient at E14 and E16 was significantly higher than that at E12 (* p=0.02, n=83 at E12, n=143 at E14, and n=46 at E16). (C) The mean duration of each $[Ca^{2+}]_i$ transient at E12 (n=40) was significantly longer than that at E14 (**p=0.0018, n=86) and E16 (**p=0.003, n=32). (D) The mean amplitude of each $[Ca^{2+}]_i$ transient at E12 (n=40) was also significantly higher than that at E14 (*p =0.0131, n=86) and E16 (*p= 0.0141, n=32). Values are mean ± SEM.

To test whether tissue damage decreased the Fluo-4 AM signal (**Figure 3.3C, F, I, Figure 3.5A**) and the amplitude of intermittent $[Ca^{2+}]_i$ transients (**Figure 3.5D**) from

E12 to E16, we analyzed their viability by monitoring mitochondrial membrane potential in the VZ using MitoTracker during calcium imaging (**Figure 3.6A–F**). We observed no significant differences in the mitochondrial membrane potential before and after imaging among the three developmental stages (data not shown). The average fluorescence intensity of MitoTracker signal within 0.004 mm^2 area in the VZ was 309.7±54.03 at E12, 380.7±75.53 at E14, and 465.3±191.1 at E16 (**Figure 3.6G**). Furthermore, we did not observe any fusion of mitochondria, which is a typical sign of apoptosis (data not shown). Although this result indicates a decrease in $[Ca^{2+}]_i$ levels from E12 to E16, it is unclear whether the intensity of the Fluo-4 AM signal accurately reflects $[Ca^{2+}]_i$ levels. However, further examination is still needed.

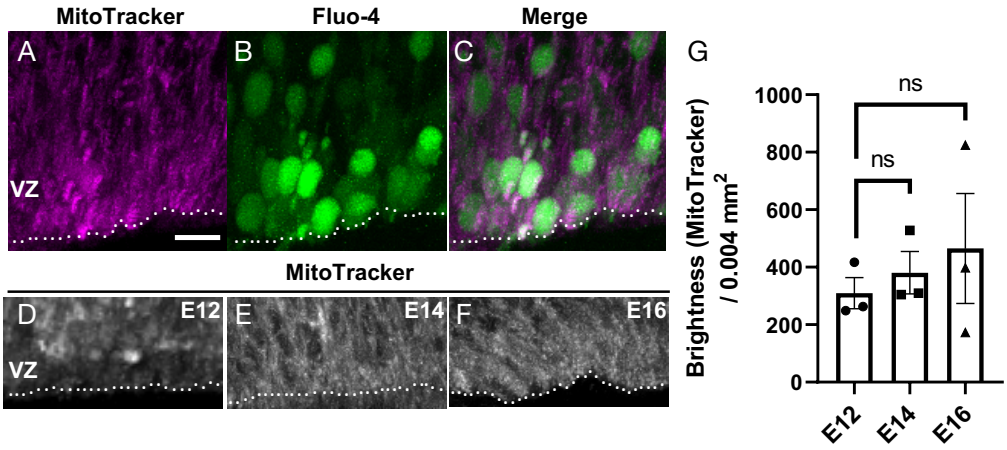

Figure 3.6 Fluorescence MitoTracker signal at E12, E14, and E16.

(A–F) To check the mitochondrial membrane potential in VZ cells, coronal brain slices were treated with MitoTracker. (C) Merged image of MitoTracker (magenta, A) and Fluo-4 AM (green, B). (D, E, F) Fluorescence signal of MitoTracker in coronal slices of brain isolated from mouse embryos at E12 (D), E14 (E), and E16 (F). Scale bar in (A) is 20 μm for (A–F). Dotted lines in (A–F) indicate the ventricular surface. (G) There was no significant difference in the average quantified fluorescence signal of MitoTracker per 0.004 mm^2 between E12, E14, and E16. Values are mean ± SEM.

3. 3. $[Ca^{2+}]_i$ fluctuations in cells isolated from the embryonic cortex

Our observations suggested that $[Ca^{2+}]_i$ levels decrease and the pattern of $[Ca^{2+}]_i$ fluctuation changes during NPC development from E12 to E16. We observed several cells with different $[Ca^{2+}]_i$ levels and fluctuation patterns at the same developmental stage (**Figure 3.3C, F, I**). This could be due to the diverse cell types in the VZ, such as NPCs and immature neurons. To understand the relationship between cell type and the level or pattern of $[Ca^{2+}]_i$ fluctuation, we identified each cell type using immunohistochemistry after recording the Fluo-4 AM signal in cells isolated from the embryonic cortex. There was no significant difference in the parameters in Fluo-4 AM signal between brain slices and the suspended cells (**Figure 3.7C)**. The frequency observed in brain slices was 0.51 ± 0.06/observation, while that in the suspended Pax6-positive cells was 0.36 ± 0.05/trial (**Figure 3.7D)**. No significant difference in the duration was observed between brain slices and suspended Pax6-positive cells (**Figure 3.7E**). Thus, the Fluo-4 AM signaling pattern in the isolated cells reproduced the pattern in mouse embryonic brain slices. However, the procedure to generate the cell suspension from the embryonic cortex may cause damage. To examine cell viability after the procedure, we detected apoptotic cells isolated from E11, E12, E14, and E16 stages using propidium iodide (PI; **Figure 3.8A-D**). Although we observed about 60% dead cells after the procedure, most cells exhibiting Fluo-4 AM signal were not apoptotic (**Figure 3.8E**), which included Pax6-positive cells.

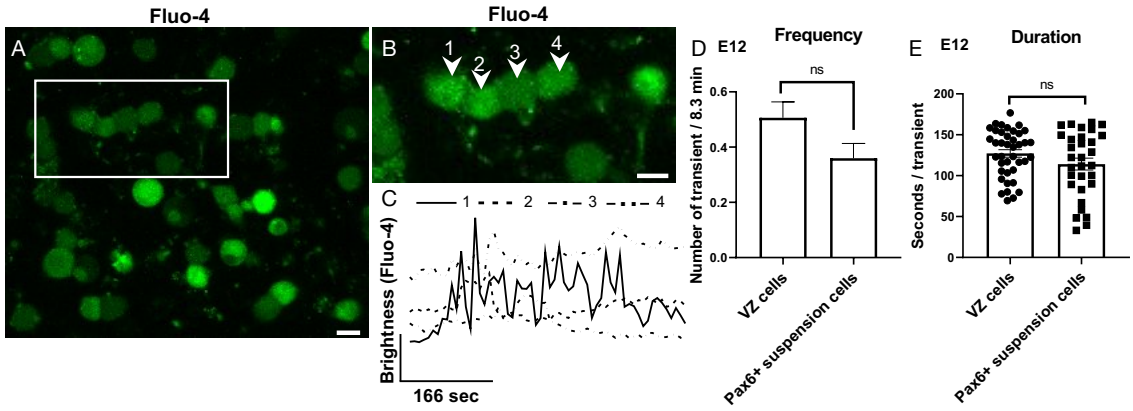

Figure 3.7 $[Ca^{2+}]_i$ fluctuations in cells isolated from the embryonic cerebral cortex.

(A) The Fluo-4 AM fluorescence signal was recorded in suspended cells. (B) High-magnification images from panel (A). Scale bar is 10 μm in (A, B). (C) Temporal changes in the fluorescence intensity of Fluo-4 AM shown by the numbered cells in (B). (D, E) There was no significant difference in the mean number of intermittent $[Ca^{2+}]_i$ transient per imaging (8.3 min) and in the duration of each intermittent $[Ca^{2+}]_i$ transient between VZ cells (n=40) and Pax6-positive suspended cells (n=31) at E12. Values are mean ± SEM.

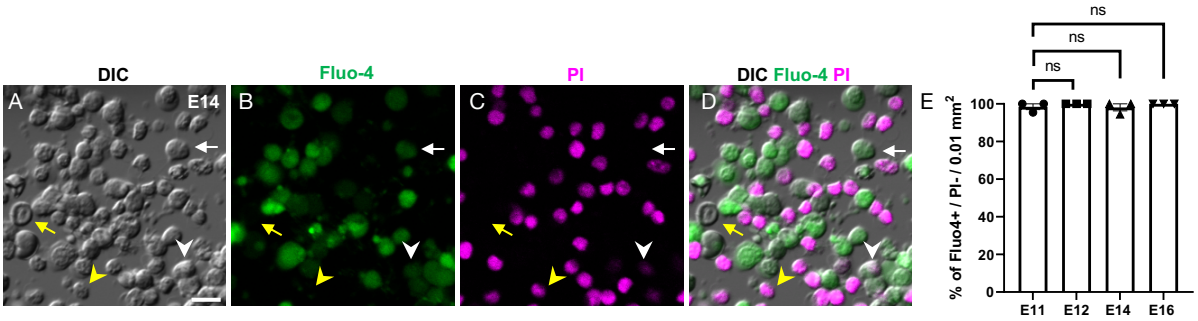

Figure 3.8. Viability of cells isolated from the embryonic cortex.

(A–D) We examined the viability of the cells isolated from the embryonic cortex using propidium iodide (PI). The cells were treated with PI (C) and then fluctuation of Fluo-4 AM signal was recorded (B). To evaluate the results of two experiments on a cell-by-cell basis: detection of dead cells by PI (C, D) and calcium imaging by Fluo-4 AM (B, D), images by differential interference contrast (DIC in A and D) were used to confirm cell location and shape. (A–D) White arrowhead indicates one example of Fluo-4 AM/PI double-positive cell. White arrow indicates example of Fluo-4 AM-positive/PI-negative cell, and yellow arrowheads indicate Fluo-4 AM-negative/PI-positive cell. Yellow arrow in (A–D) indicates Fluo-4 AM/PI double-negative cell. About 60% of

cells were dead or dying during the procedure, but no difference was observed in the percentage of living cells exhibiting $[Ca^{2+}]_i$ fluctuations at all stages, and almost 100% cells exhibiting $[Ca^{2+}]_i$ fluctuations were living (E). Scale bar in (A) is 20 μm for (A– D). Values are mean ± SEM.

3.4 Pattern of $[Ca^{2+}]_i$ fluctuations in Pax6-positive NPCs during development.

We first focused on the Fluo-4 AM signal fluctuation pattern in Pax6-expressing cells because Pax6 plays essential roles in both proliferation and differentiation in developing NPCs (**Figure 3.9A, B**) (Estivill-Torrus et al., 2002; Quinn et al., 2007; Sansom et al., 2009). Approximately 74.9% of the Pax6-positive cells at E11 and E12 did not display intermittent $[Ca^{2+}]_i$ transients (**Figure 3.9C, D, E, Figure 3.10B**), while the number of Pax6-positive cells displaying the transients increased at E14 and E16 (**Figure 3.9C, F, G, Figure 3.10B**).

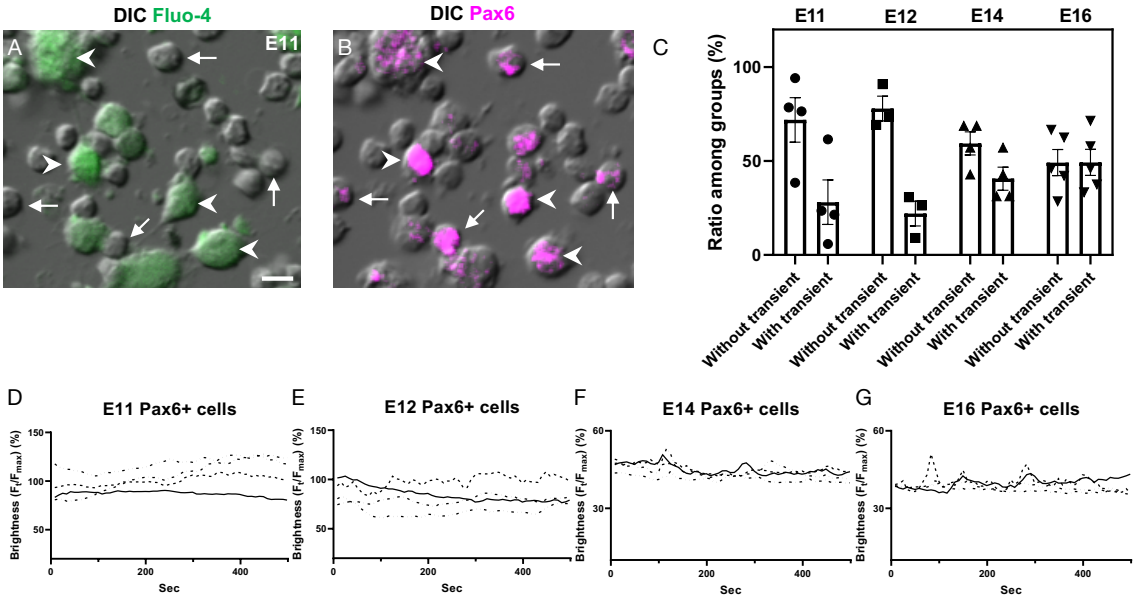

Figure 3.9. $[Ca^{2+}]_i$ fluctuations in Pax6-expressing cells.

(A, B) To characterize $[Ca^{2+}]_i$ fluctuations in developing NPCs, we detected Pax6 protein by immunostaining after recording Fluo-4 AM signal in suspended cortical cells isolated from mouse embryos at E11, E12, E14, and E16. We focused on cells with Fluo-4 AM signal (A) and Pax6 protein expression (B). Arrowheads indicate Pax6/Fluo-4 AM double-positive cells, and arrow indicate Pax6-positive/Fluo-4 AM-negative cells in (A, B). Scale bar is 10 μm for (A, B). (C) The ratio (among the two groups) based on the pattern of temporal change in Fluo-4 AM signal in each stage showed that the dominant pattern of $[Ca^{2+}]_i$ fluctuation was without intermittent $[Ca^{2+}]_i$ transient at E11 and E12. In contrast, the cells exhibiting $[Ca^{2+}]_i$ fluctuation with $[Ca^{2+}]_i$ transients were increased at E14 and E16. (D–G) Fluctuation patterns of Fluo-4 AM signaling in Pax6-positive cells at E11 (D), E12 (E), E14 (F), and E16 (G). Values are mean ± SEM.

The mean Fluo-4 AM signal in Pax6-expressing cells of E11 and E12 embryos was significantly higher than that of E14 and E16 embryos (**Figure 3.9D-G, Figure 3.10A**). However, no significant difference was observed in the duration and amplitude of individual $[Ca^{2+}]_i$ transients at E12, E14, and E16 (**Figure 3.10C, D**).

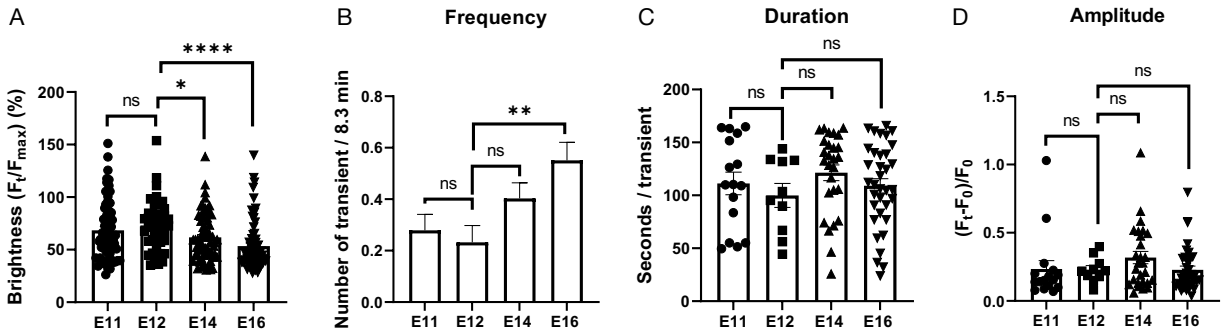

Figure 3.10. Fluo-4 AM intensity, frequency, duration, and amplitude transient in Pax6-positive cell $[Ca^{2+}]_i$ fluctuations.

(A) Average intensity of Fluo-4 AM signal per cell was indicated by the value of brightness (Ft/F_{max}) in Pax6-positive cells at E11, E12, E14, and E16. No significant difference was observed in the value of brightness (Ft/F_{max}) between E11 (n=61) and E12 (n=43). The value of brightness (Ft/F_{max}) in the cells that isolated from E12 was significantly higher than that at E14 (*p=0.012, n=67) and E16 (****p <0.0001, n=69). (B) The mean number of intermittent $[Ca^{2+}]_i$ transients per observation. From E12 to E16, the average number of intermittent $[Ca^{2+}]_i$ transients appeared to increase (**p=0.0025). The mean number of the transients was highest at E16. (C) The mean duration of each intermittent $[Ca^{2+}]_i$ transient was not significantly different among E11 (n=16), E12 (n=10), E14 (n=27), and E16 (n=35). (D) The mean amplitude of each intermittent $[Ca^{2+}]_i$ transient was also not significantly different among E11, E12, E14, and E16. Values are mean ± SEM.

The observed difference in the pattern of Fluo-4 AM signal fluctuation and average Fluo-4 AM signal levels was consistent with the difference observed in the VZ region of embryonic brain slices (**Figure 3.5A, Figure 3.10A**), suggesting that the pattern of $[Ca^{2+}]_i$ fluctuation in Pax6-positive cells changed from E11 to E16. The number of intermittent $[Ca^{2+}]_i$ transients seemed to increase gradually, while the $[Ca^{2+}]_i$ gradually decreased, which is consistent with the results from brain slices. Thus, the generation of intermittent $[Ca^{2+}]_i$ transients may be associated with the differentiation of self-renewing NPCs into neuron-generating NPCs or immature neurons.

3.5 $[Ca^{2+}]_i$ fluctuations in immature neurons

More than 70% of the Pax6-positive cells at E11 and E12 exhibited $[Ca^{2+}]_i$ fluctuations without intermittent $[Ca^{2+}]_i$ transients (**Figure 3.9C**). In contrast, more Pax6-positive cells displayed intermittent $[Ca^{2+}]_i$ transients at E16 (**Figure 3.9C**). Thus, we examined whether immature neurons (Tuj1-positive cells) exhibited more intermittent $[Ca^{2+}]_i$ transients. We characterized the Fluo-4 AM signal pattern of Tuj1-positive cells by identifying Tuj1-positive cells after imaging (**Figure 3.11A, B, F**). At E11, the proportion of a population of Pax6-positive NPC was 32.4%, while Tuj1-positive neurons were 15.1% (**Figure 3.11C)**. Surprisingly, more than half of the Tuj1-positive cells showed intermittent $[Ca^{2+}]_i$ transients in Fluo-4 AM signaling, while 25% of Pax6-positive cells exhibited the transients (**Figure 3.11D, E, F, H**). No noticeable difference was observed in the duration and amplitude of each intermittent $[Ca^{2+}]_i$ transient between the two cell types (**Figure 3.11I, J**). The average Fluo-4 AM signal in Tuj1-positive cells was significantly lower than that in Pax6-positive cells (F_t / F_{max} in Pax6-positive cells, 68.35 ± 3.6; in Tuj1-positive cells, 24.63 ± 1.18, **Figure 3.11G**). The decrease in the $[Ca^{2+}]_i$ and generation of intermittent $[Ca^{2+}]_i$ transients may be coupled with the differentiation of Pax6-positive cells into Tuj1-positive immature neurons.

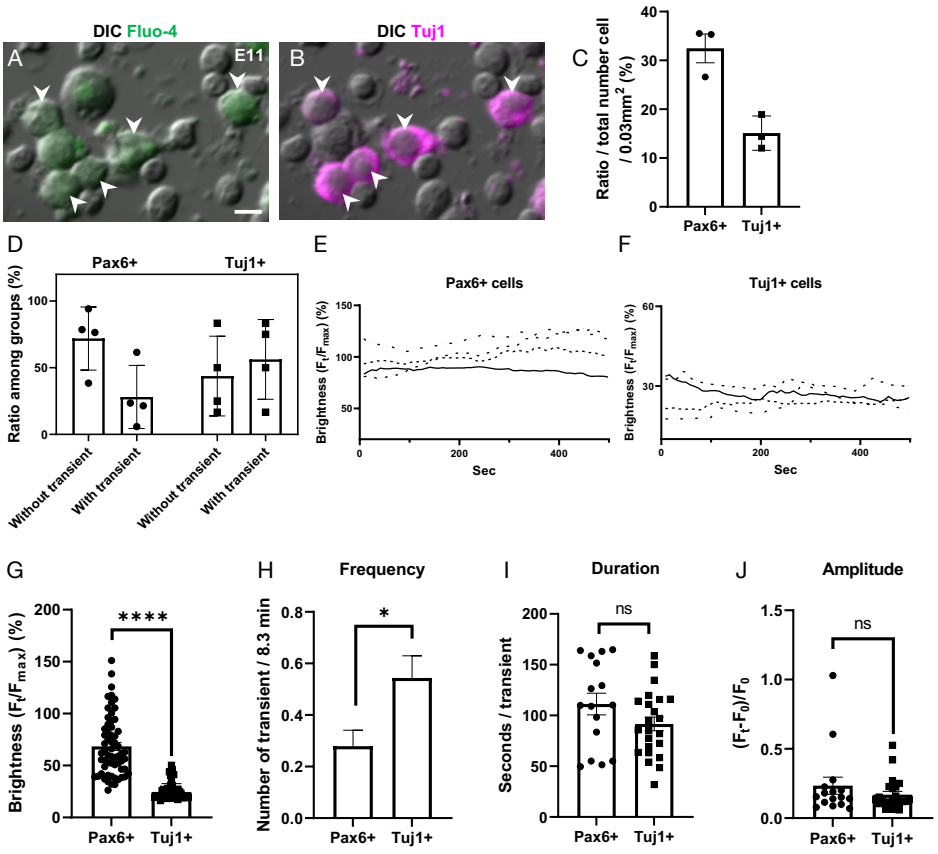

Figure 3.11. $[Ca^{2+}]_i$ fluctuations in immature neurons.

(A, B) To characterize $[Ca^{2+}]_i$ fluctuation in immature neurons, we detected Tuj1 proteins by immunostaining after recording Fluo-4 AM signal from cortical cells isolated from mouse embryos at E11. We detected the cells expressing Tuj1 (magenta, B) and those exhibiting Fluo-4 AM signal fluctuations (A). Arrowheads indicate Tuj1-expressing immature neurons exhibiting Fluo-4 AM signal fluctuation in (A, B). Scale bar in (A) is 10 μm for (A, B). (C) Proportion of population in Pax6-positve and Tuj1-positive cells. (D) 56 % of the Tuj1-positive cells showed intermittent $[Ca^{2+}]_i$ transients, while only about 28 % of the Pax6-positive cells showed the transients. (E, F) Representative temporal change in Fluo-4 AM signal recorded in Pax6-positive (E), and Tuj1-positive cells at E11 (F). (G) Average intensity of Fluo-4 AM signal in the Pax6-positive cells (n= 61) was significantly higher than in Tuj1-positive cells (****p<0.0001, n=46). (H) The mean number of intermittent $[Ca^{2+}]_i$ transients per observation in Pax6-positive cells were less than those in Tuj1-positive cells (*p=0.012). (I) No significant difference was observed in the duration of each intermittent $[Ca^{2+}]_i$ transient between Pax6-positive (n=16), and Tuj1-positive cells (n=23). (J) No significant difference was found in the amplitude of each intermittent $[Ca^{2+}]_i$ transient between both cell types. Values are mean ± SEM.

3.6 $[Ca^{2+}]_i$ fluctuation in self-renewing undifferentiated and neuron-generating Pax6-positive cells

More than half of Tuj1-positive immature neurons exhibited intermittent $[Ca^{2+}]_i$ transients, whereas only 28% of Pax6-positive cells exhibited the transients at E11 (**Figure 3.11C**). This result suggested that the onset of the intermittent $[Ca^{2+}]_i$ transients may be a hallmark of change toward more differentiated cells. Since the initiation of Btg2 expression in Pax6-positive cells is known to trigger neuronal differentiation, we investigated whether the onset of intermittent $[Ca^{2+}]_i$ transients correlated with the initiation of Btg2 expression (Canzoniere et al., 2004; Farioli-Vecchioli et al., 2009; Farioli-Vecchioli et al., 2008; Farioli-Vecchioli et al., 2007; Iacopetti et al., 1994; Iacopetti et al., 1999). Btg2-positive cells were only 26% among Pax6-positive cells at E11 and were 53% at E14, suggesting that more Pax6-positive cells are committed to differentiation at E14 (**Figure 3.12A–E**).

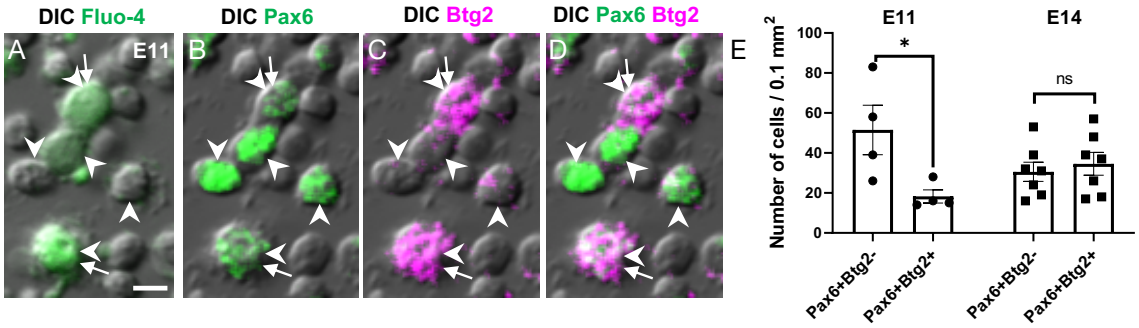

Figure 3.12. Self-renewing undifferentiated and neuron-generating Pax6-positive cells.

(A–D) To characterize $[Ca^{2+}]_i$ fluctuations in undifferentiated and neuron-generating Pax6-positive cells, we detected Pax6 (B) and Btg2 protein (C) by immunostaining after recording Fluo-4 AM signal (A) from suspended cortical cells isolated from mouse embryos at E11 and E14. Merged image of Pax6 (green) and Btg2 (magenta) is shown in (D). Arrowheads in (A–D) indicate Pax6-positive cells, and arrows indicate Btg2-positive cells. Scale bar in (A) is 10 μm for (A–D). (E) The number of Pax6-positive/Btg2-negative cells was about three times more than that of Pax6/Btg2 double-positive cells per 0.1 mm^2 at E11, whereas no significant difference was observed between Pax6-positive/Btg2-negative cells and Pax6/Btg2 double-positive cells at E14. Values are mean ± SEM.

Interestingly, the number of intermittent $[Ca^{2+}]_i$ transients in the Pax6/Btg2 double-positive cells at E11 was 0.36 ± 0.08, while that in the Pax6-positive/Btg2-negative cells was 0.1 ± 0.06 (**Figure 3.13A, B, F**). In addition, we observed that only 13% of the Pax6-positive/Btg2-negative cells showed the $[Ca^{2+}]_i$ transients, whereas almost 40% of Pax6/Btg2 double-positive cells exhibited intermittent $[Ca^{2+}]_i$ transients (**Figure 3.13E),** indicating that more cells displayed intermittent $[Ca^{2+}]_i$ transients among Pax6/Btg2 double-positive cells. In contrast, no significant difference was observed in the number and intensity of intermittent $[Ca^{2+}]_i$ transients between both cell types at E14 (**Figure 3.13C-F).** These results suggested that more Pax6-positive cells at E14 are committed to differentiation compared to those at E11, and the onset of intermittent $[Ca^{2+}]_i$ transients may accompany their differentiation. No significant

difference was observed in Fluo-4 AM signal levels between Pax6-positive/Btg2-negative cells and Pax6/Btg2 double-positive cells at E11 and E14 (**Figure 3.13G**).

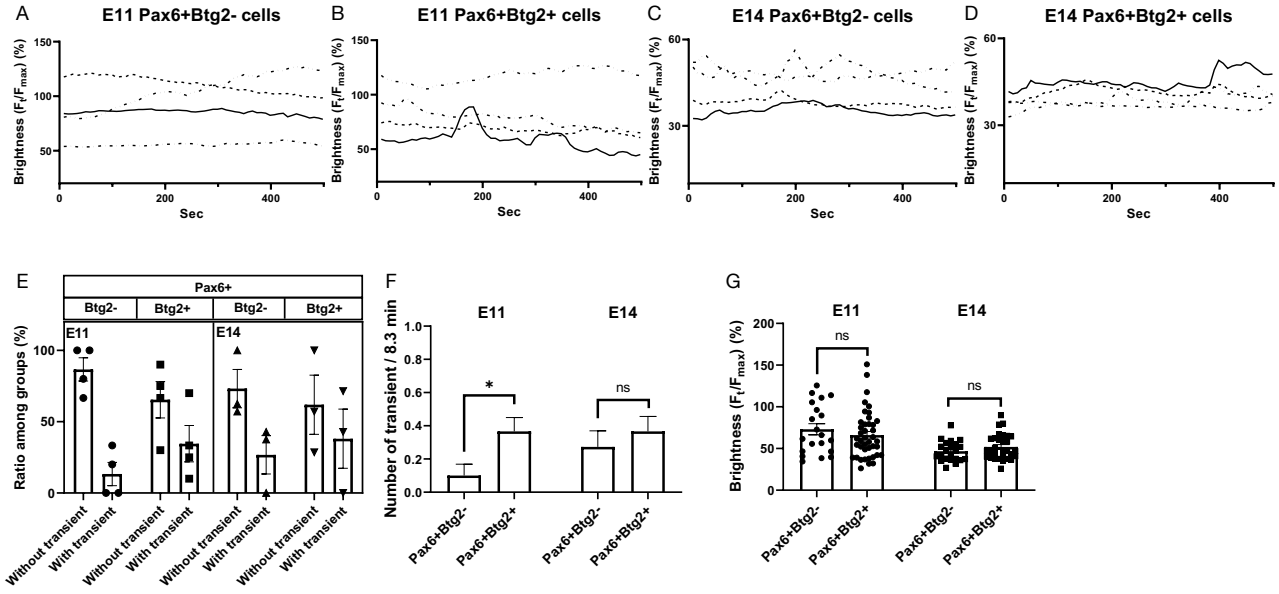

Figure 3.13. $[Ca^{2+}]_i$ fluctuation in undifferentiated and neuron-generating Pax6-positive cells.

(A–D) Example of temporal change pattern in Fluo-4 AM signal in Pax6-positive/Btg2-negative cells at E11 (A), Pax6/Btg2 double-positive cells at E11 (B), Pax6-positive/Btg2-negative cells at E14 (C), and Pax6/Btg2 double-positive at E14 (D). (E) The ratio among the two groups based on the pattern of temporal change in Fluo-4 AM signal in Pax6-positive/Btg2-negative cells and Pax6/Btg2 double-positive cells at E11 and E14. At E11, more Pax6/Btg2 double-positive cells exhibited intermittent $[Ca^{2+}]_i$ transients than Pax6-positive/Btg2-negative cells. There was no significant difference in both cell types at E14. (F) More Pax6/Btg2 double-positive cells showed intermittent $[Ca^{2+}]_i$ transients than Pax6-positive/Btg2-negative cells at E11 (*p=0.044, n=20 Pax6-positive/Btg2-negative cells, n=41 Pax6/Btg2 double-positive cells). No significant difference was observed in the number of cells displaying $[Ca^{2+}]_i$ transients between the two groups at E14 (n=22 for Pax6-positive/Btg2-negative cells, n=30 for Pax6/Btg2 double-positive cells). (G) No significant difference was observed in the average intensity of Fluo-4 AM signal between Pax6-positive/Btg2-negative cells and Pax6/Btg2 double-positive cells at E11 and E14. Values are mean ± SEM.

3.7 Mechanisms of $[Ca^{2+}]_i$ fluctuations observed in the VZ

It has been reported that the majority of $[Ca^{2+}]_i$ fluctuations in the rat cortical VZ at E15 and E19 are mediated by Ca^{2+} release from intracellular stores (Owens & Kriegstein, 1998). To examine if our observation using Fluo-4 AM at E12–16 was due to the same mechanism, we performed imaging experiments using cortical slices treated with 5 μM thapsigargin. Surprisingly, no noticeable effect of thapsigargin on the Fluo-4 AM signal was observed (**Figure 3.14A-D**). To test whether the fluctuations in Fluo-4 AM signal were mediated by extracellular calcium, we examined the effect of 5 mM EGTA on the fluctuations. We observed that the Fluo-4 AM signal was significantly reduced by 5 mM EGTA treatment (**Figure 3.15A, B, F, G**), indicating that the observed fluctuation of Fluo-4 AM signal is mediated by the influx of extracellular calcium. To identify the calcium channel, we examined the effects of several inhibitors for calcium channels. Treatment with 20 μM nifedipine, an inhibitor of L-type calcium channels, had a slight inhibitory effect on the fluctuation of Fluo-4 AM signal (**Figure 3.15C, H, I**). In addition, 10 μM mibefradile, a potent inhibitor of both T-type and L-type channels (Martin et al., 2000), also slightly reduced the number of cells exhibiting Fluo-4 AM signal fluctuations with intermittent $[Ca^{2+}]_i$ transients (**Figure 3.15D, H, I**). In contrast, 2.5 μM NNC 55-0396, which is a specific inhibitor of T-type calcium channels in Cav3.1 and Cav3.2 (Huang et al., 2004; Taylor et al., 2008), significantly blocked the fluctuations of Fluo-4 AM signal (**Figure 3.15E, H, I**), suggesting that the $[Ca^{2+}]_i$ fluctuations observed in the VZ at E12 are mediated by T-type calcium channels.

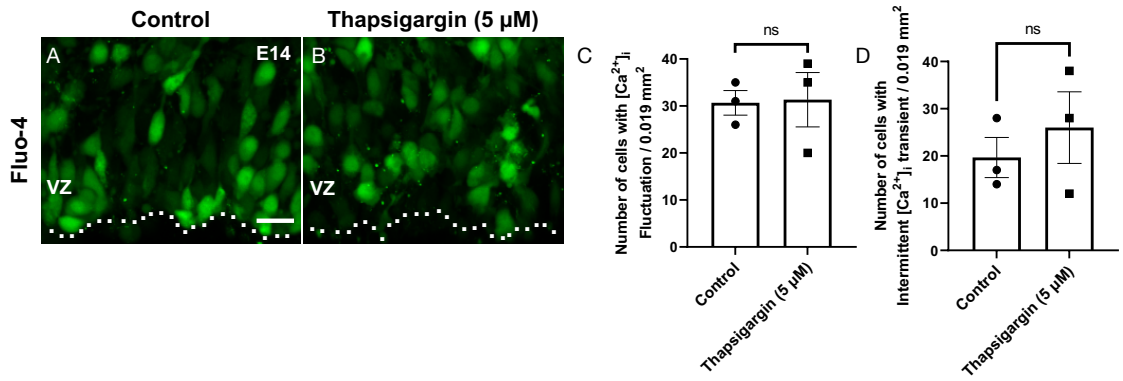

Figure 3.14. Mechanism of $[Ca^{2+}]_i$ fluctuations in the cortical VZ region (1).

(A-B) The fluorescent Fluo-4 AM signal was recorded in the VZ at E14 as a control (A), in medium contain 5 µM Thapsirgargin (B). Scale bar in (A) is 20 µm for (A,B). Dotted lines in (A,B) indicate the ventricular surface. (B, F, G) Fluo-4 AM signal in calcium-free medium (B), (C-D) There is no significant different in the number of cells with Fluo-4 AM signal between in the Thapsirgargin and in the control (C), also, there was no significant difference in the number of cells exhibiting fluctuations with intermittent $[Ca^{2+}]_i$ transients between the control and medium containing 5 µM Thapsirgargin (D). Values are mean ± SEM.

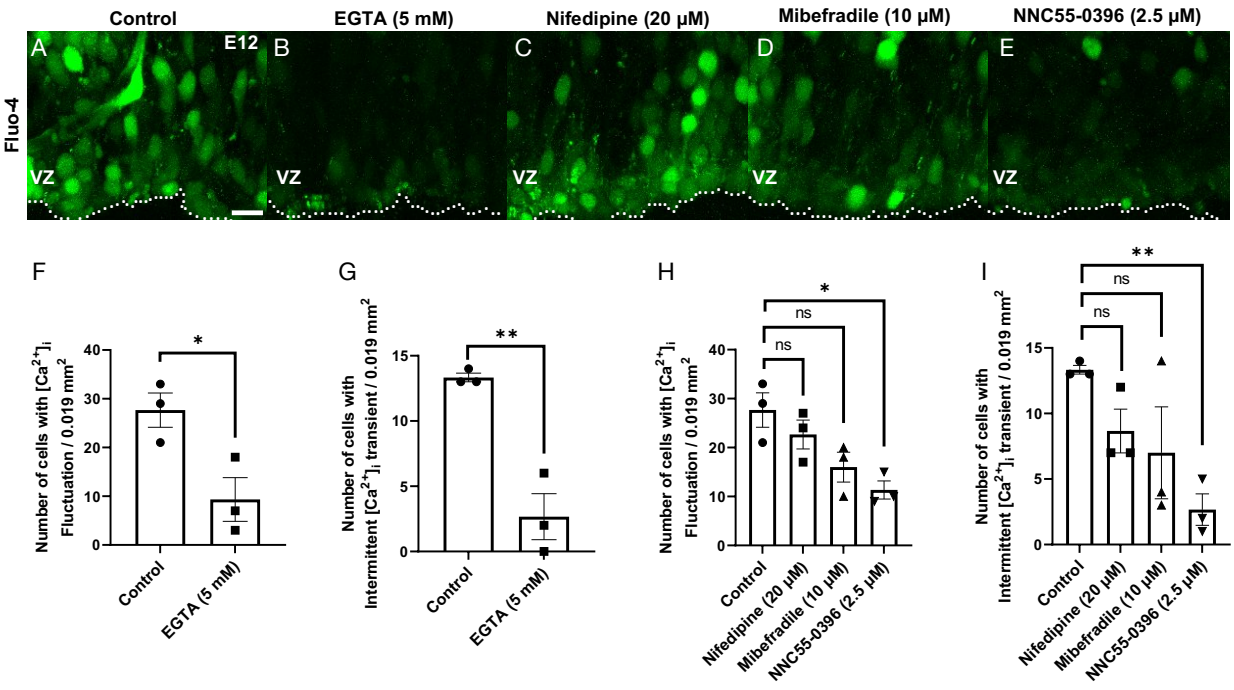

Figure 3.15. Mechanism of $[Ca^{2+}]_i$ fluctuations in the cortical VZ region (2).

(A–E) The fluorescent Fluo-4 AM signal was recorded in the VZ at E12 as a control (A), in calcium-free (0 M Ca^{2+} and 5 mM EGTA) medium (B), and in medium containing 20 μM nifedipine (C), 10 μM mibefradile (D), and 2.5 μM NNC55-0396 (E). Scale bar in (A) is 20 μm for (A–E). Dotted lines in (A–E) indicate the ventricular surface. (B, F, G) Fluo-4 AM signal in calcium-free medium (B), indicating fewer number of cells with Fluo-4 AM signal in calcium-free medium per 0.019 mm^2 than that in the control (*p =0.0325) (B, F), and the cells showing fluctuation with intermittent $[Ca^{2+}]_i$ transients were more affected by the calcium-free conditions (**p =0.004) (B, G). (C, D, E, H) The mean number of cells with Fluo-4 AM signal fluctuations between the medium containing 20 μM nifedipine, 10 μM mibefradile, and 2.5 μM NNC55-0396 was compared to that in the control. In the medium containing 2.5 μM NNC55-0396, the mean number of cells with Fluo-4 AM signal was significantly reduced (*p =0.0149) (E, H), while the effect of 20 μM nifedipine (C, H) and 10 μM mibefradile (D, H) did not show a significant reduction. (I) The mean number of cells exhibiting fluctuation with intermittent $[Ca^{2+}]_i$ transient was also significantly reduced in the medium containing 2.5 μM NNC55-0396 (**p=0.001). There was no significant difference in the number of cells exhibiting fluctuations with intermittent $[Ca^{2+}]_i$ transients between the control and medium containing 20 μM nifedipine or 10 μM mibefradile (I). Values are mean ± SEM.

Next, to confirm whether the fluctuation of the Fluo-4 AM signal in Pax6-positive cells were also mediated by T-type calcium channels, we examined the effect of 2.5 μM NNC 55-0396. Consistent with the results in the embryonic slices (**Figure 3.16E, H, I**), the intermittent $[Ca^{2+}]_i$ transients in Pax6-positive cells at E14 were significantly inhibited by treatment with NNC55-0396 (**Figure 3.16A, B**). These results suggested that T-type calcium channels could be involved in the intermittent $[Ca^{2+}]_i$ transients in Pax6-positive cells during their differentiation into a neurogenic state.

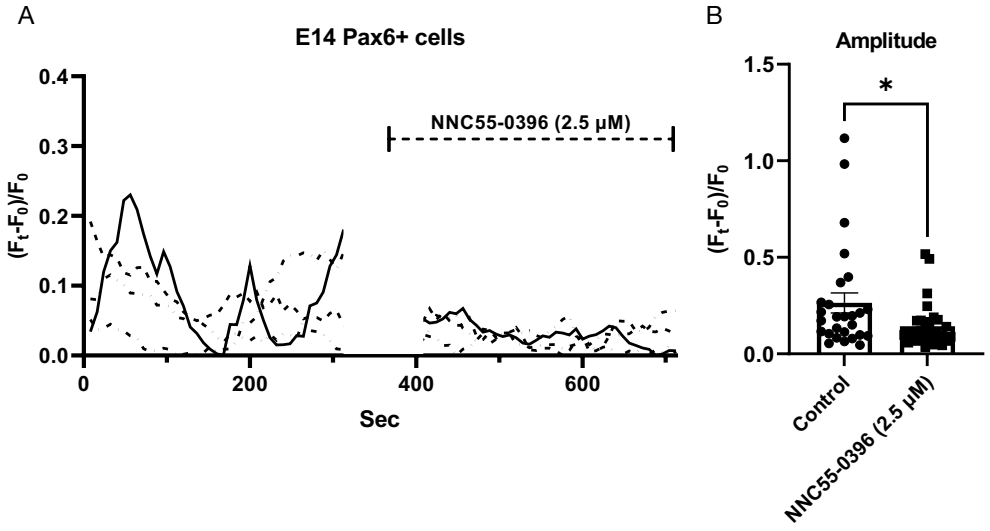

Figure 3.16. Mechanism of $[Ca^{2+}]_i$ fluctuations in Pax6-positive cells.

(A) The observed intermittent $[Ca^{2+}]_i$ transients in Pax6-positive cells at E14 was inhibited by treatment with 2.5 μM NNC55-0396. (B) The average amplitude of the $[Ca^{2+}]_i$ transients was also reduced by treatment with NNC55-0396 (*p=0.02, n=30). Values are mean ± SEM.

3. 8 Inhibiting $[Ca^{2+}]_i$ fluctuations in neurosphere culture

Our results suggested that the increased number of intermittent $[Ca^{2+}]_i$ transients may correlate to the differentiation of Pax6-positive cells. To examine the relation between

$[Ca^{2+}]_i$ fluctuations and neural differentiation of NPCs, we inhibited $[Ca^{2+}]_i$ fluctuations in NPCs by treatment with NNC 55-0396 in neurosphere cultures. The number of neurospheres in the group treated with 2.5 μM NNC 55-0396 was almost 25% more than that in the control group (**Figure 3.17A, C, E**), but was not affected by treatment with 1 μM NNC 55-0396 (**Figure 3.17A, B, E**). The number of spheres in the group treated with 5 μM NNC 55-0396 was significantly decreased (**Figure 3.17A, D, E, F, G**). However, we do not know precisely how high doses of NNC 55-0396 cause the neurosphere to fail to form. It may be because T-type calcium channels are also associated with survival in NPCs (Kim et al., 2018). The number of spheres smaller than 100 μm in diameter was increased after treatment with 2.5 μM NNC 55-0396, but the number of spheres larger than 100 μm in diameter was not affected (**Figure 3.17F, G**). In contrast, treatment with 1 μM NNC 55-0396 increased the number of spheres larger than 100 μm in diameter (**Figure 3.17B, G**), suggesting that the inhibition of $[Ca^{2+}]_i$ fluctuations by 2.5 μM NNC 55-0396 maintains cell survival and enhances cell proliferation. If treatment with NNC 55-0396 promotes cell survival or NPC proliferation, the number of secondary spheres should be higher than in controls. As expected, the number of secondary spheres after treatment with 2.5 μM NNC 55-0396 was 16% more than that in controls, suggesting that inhibition of $[Ca^{2+}]_i$ fluctuations enhance cell survival or cell proliferation (**Figure 3.17H**).

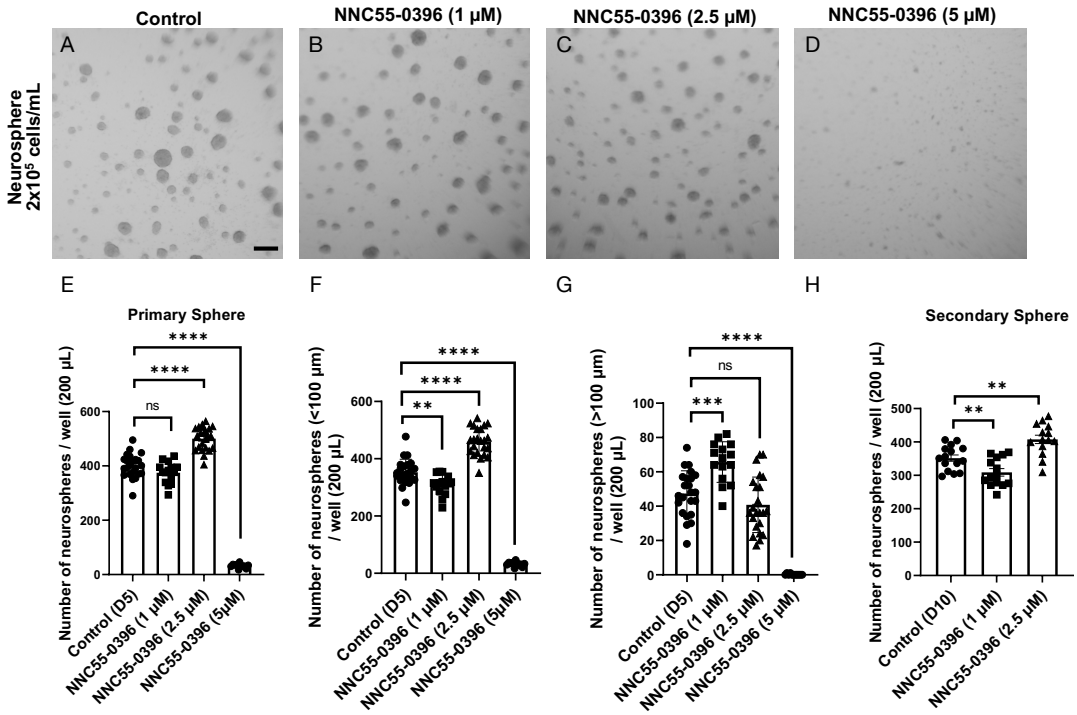

Figure 3.17. Inhibiting $[Ca^{2+}]_i$ fluctuations increases neurospheres.

(A–D) Neurospheres formed after five days of culture of suspended cells isolated from embryonic cortex at E12 (A), neurospheres in the culture medium containing 1 μM NNC55-0396 (B), neurospheres in culture medium containing 2.5 μM NNC55-0396 (C), and neurospheres in culture medium containing 5 μM NNC55-0396 (D). Scale bar in (A) is 400 μm for (A–D). (E) The mean number of primary neurospheres in the control, in medium containing 1 μM NNC55-0396, in medium containing 2.5 μM NNC55-0396, and in medium containing 5 μM NNC55-0396. The mean number of primary neurospheres was increased in medium containing 2.5 μM NNC55-0396 (****p<0.0001, n=23), and significantly reduced in the medium containing 5 μM NNC55-0396 (****p<0.0001, n=11). There was no significant difference between the control (n=23) and the group treated with 1 μM NNC55-0396 (n=15). (F) The mean number of neurospheres < 100 μm in diameter was increased in the medium containing 2.5 μM NNC55-0396 (****p<0.0001), but was slightly decreased after treatment with 1 μM NNC55-0396 (**p=0.003), and significantly reduced in the medium containing 5 μM NNC55-0396 (****p<0.0001). (G) The mean number of neurospheres more than 100 μm in diameter was increased by treatment with 1 μM NNC55-0396 (***p=0.0001), but significantly reduced in the medium containing 5 μM NNC55-0396 (****p<0.0001). There was no significant difference in the number between the control and the 2.5 μM NNC55-0396 groups. (H) The mean number of secondary neurospheres was also increased by treatment with 2.5 μM NNC55-0396 (**p=0.0013, n=14), but was decreased by 1 μM NNC55-0396 (**p= 0.007), compared to that in the control (n=15). Values are mean ± SEM.

If the inhibition of $[Ca^{2+}]_i$ fluctuations enhances NPC proliferation, their differentiation could be suppressed. To test this hypothesis, we examined the number of Tbr1-positive cells in the spheres approximately 100 μm in diameter formed after treatment with 2.5 μM NNC 55-0396. Tbr1 is a marker of immature postmitotic projection neurons (Bedogni et al., 2010; Englund et al., 2005). Thus the number of Tbr1-positive cells was expected to decrease if the self-duplication of NPCs was enhanced. The number of Tbr1-positive cells in the group treated with 2.5 μM NNC 55-0396 was 14.2 ± 2.03/sphere, which was approximately half of that in control (29.36 ± 2.98/sphere) (**Figure 3.18A, B, C**). The number of Tbr1-positive cells per sphere with 1 μM NNC 55-0396 was 22.29 ± 2.37/sphere, which was slightly lower but not significantly different from that in control (**Figure 3.18C**). Thus, these results suggested that inhibiting the T-type calcium channels in NPCs enhances their proliferation and inhibits neural differentiation.

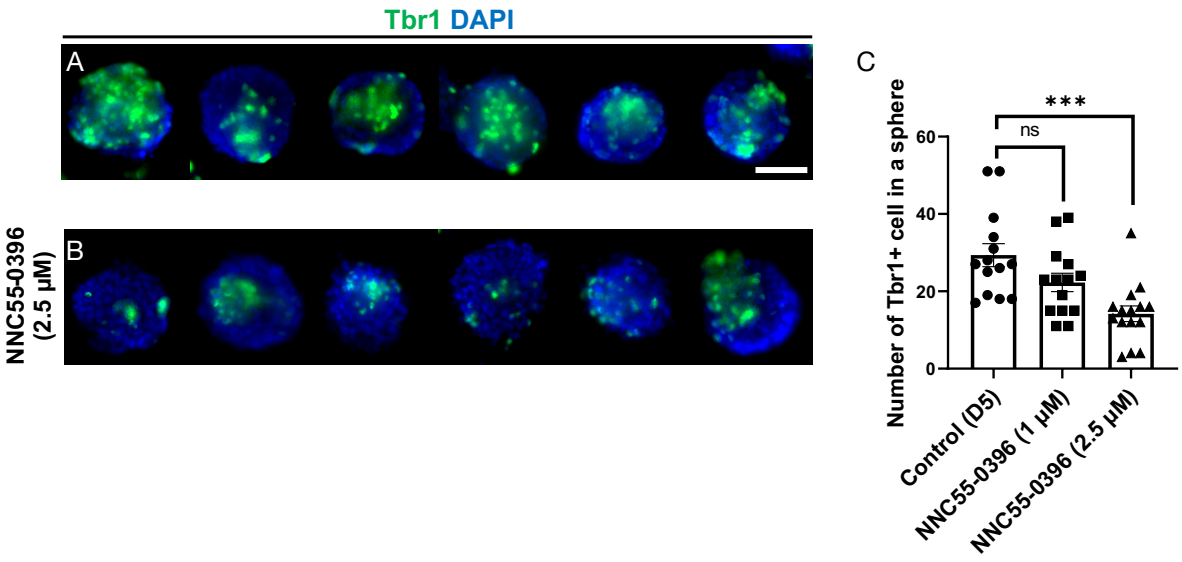

Figure 3.18. Inhibiting $[Ca^{2+}]_i$ fluctuations impairs neural differentiation.

Neuronal differentiation in neurospheres was analyzed using Tbr1 protein after five days of culture in control (A), and after treatment with 2.5 μM NNC55-0396 (B); DAPI+ (blue) and Tbr1+ cell (green). Scale bar in (A) is 50 μm for (A,B). (C) The number of Tbr1-positive cells in neurospheres after treatment with 2.5 μM NNC55-0396 was reduced compared (***p=0.0002, n=15) to that in the control (n=14). No significant difference was observed between the control and the group treated with 1 μM NNC55-0396 (n=14). Values are mean ± SEM.

3. 9 *In vivo* knockdown of T-type Ca^{2+} channel expression

$[Ca^{2+}]_i$ fluctuations mediated by T-type calcium channels may be required for the neural differentiation of NPCs. To investigate this possibility *in vivo*, we inhibited the expression of the T-type calcium channel in NPCs *in vivo* using RNAi and examined the cell-autonomous effect of inhibiting T-type calcium channels on NPC differentiation. Three subtypes of T-type calcium channels, Cav3.1 (encoded by Cacna1g), Cav3.2 (encoded by Cacna1h), and Cav3.3 (encoded by Cacna1i), have been identified (Aguado et al., 2016; Yunker et al., 2003), and Cav3.1 is expressed in NPCs (Kim et al., 2020; Kim et al., 2018; Yabuki et al., 2021). To inhibit Cav3.1 expression

in developing cortical NPCs, we introduced an RNAi expression vector for Cav3.1 together with a GFP expression vector into cortical VZ cells at E14.5 using *in-utero* electroporation. At 24 h after electroporation, we examined whether the GFP-positive cells expressed Pax6 or Tbr1. In cells transfected with the control vector, the proportion of Pax6-positive cells and Tbr1-positive cells was similar (Pax6-positive cells, 44.9 ± 2.86%; Tbr1-positive cells, 53.38 ± 2.61%, **Figure 3.19A, B, C, D, I**). In contrast, among cells with Cav3.1 knockdown, the proportion of Pax6-positive cells was significantly more than that of Tbr1-positive cells (Pax6-positive cells, 65.82 ± 3.88%; Tbr1-positive cells, 33.78 ± 2.59%, **Figure 3.19E, F, G, H, J**). The number of cells incorporated with the control vector was 77.3 ± 5.63/0.03 mm^2 (n=10), and that of cells with Cav3.1 knockdown vector was 93.4 ± 7.99/0.03 mm^2 (n=9) at 24 h after electroporation, respectively, indicating that Cav3.1 knockdown did not impair cell proliferation and survival. These results suggested that Cav3.1 knockdown maintains NPCs as Pax6-positive cells, resulting in a reduced proportion of Tbr1-positive cells. Thus, $[Ca^{2+}]_i$ fluctuation seems to be required for NPC differentiation into neuronal cell. Moreover, Cav3.2 knockdown did not affect NPC differentiation (**Figure 3.20**).

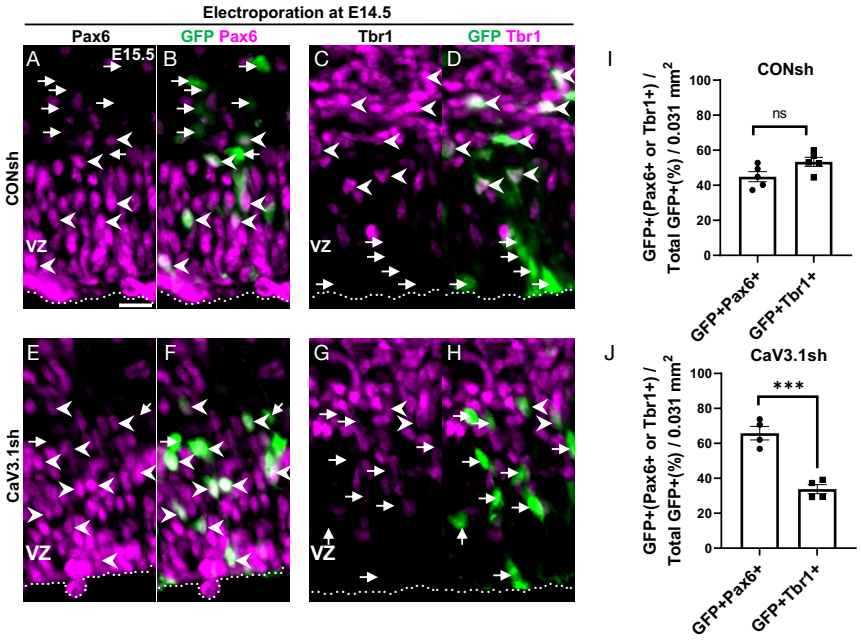

Figure 3.19. *In vivo* knockdown of Cav3.1 maintains NPCs as Pax6-expressing cells.

(A–H) To examine the role of Cav3.1 in the differentiation of VZ cells, we transfected control vector (CONsh, A–D) and shRNA vector targeting the Cav3.1 gene (Cav3.1sh, E–H) into VZ cells using *in utero* electroporation at E14.5 and observed the effect on their development at E15.5. The expression vector for GFP (green in B, D, F, H) was also transfected together with CONsh or Cav3.1sh to detect the cells containing CONsh or Cav3.1sh. (A, B, I) At 24 h after transfection of CONsh, half of the GFP-expressing cells (green) expressed Pax6 (magenta) simultaneously (arrowheads in A, B). The other half of the GFP-expressing cells (green) expressed Tbr1 (magenta) (arrowheads in C, D). In contrast, 66 % of cells containing Cav3.1sh (green in F and H) were Pax6-positive (magenta) (arrowheads in F), while only about 34 % of cells containing Cav3.1sh were Tbr1-positive (magenta in H). Note that more cells containing Cav3.1sh were localized in the VZ without expressing Tbr1 (arrows in H). (J) There was a significant reduction of GFP/Tbr1 double-positive cells per 0.031 mm^2 in Cav3.1sh (***p=0.0005), indicating a decrease in the neural differentiation from Pax6-positive cells into Tbr1-positive cells. Dotted lines in (A–H) indicate the ventricular surface. Scale bar in (A) is 20 μm for (A–H). Values are mean ± SEM.

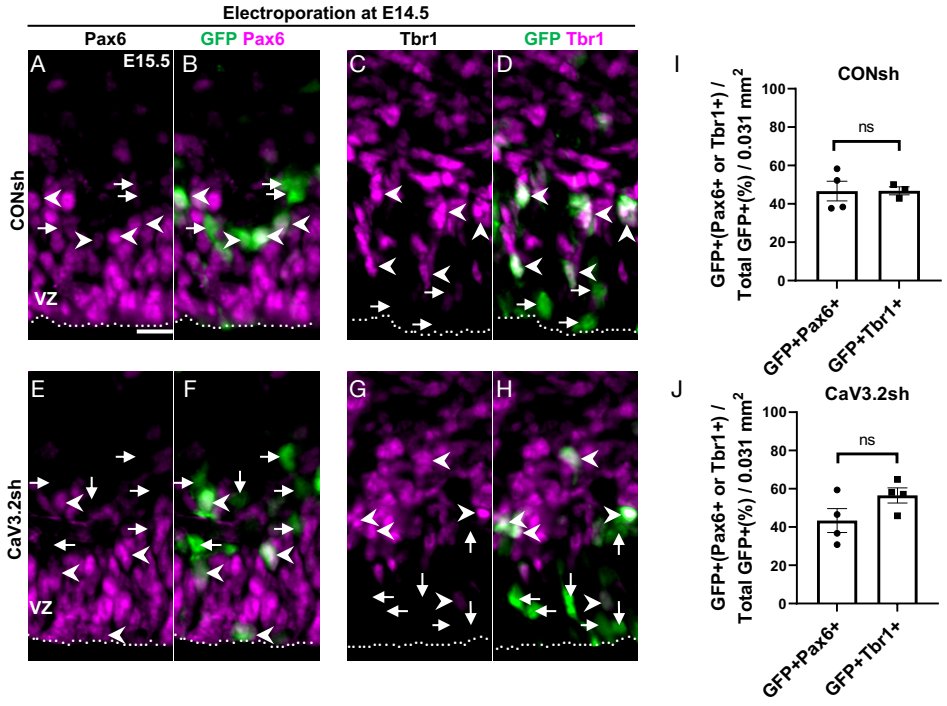

Figure 3.20. *In vivo* knockdown of Cav3.2 has no effect on neural differentiation.

(A–H) To examine the role of Cav3.2 in the differentiation of VZ cells, we transfected control vector (CONsh, A–D) and shRNA vector targeting the Cav3.2 gene (Cav3.2sh, E–H) into VZ cells using *in utero* electroporation at E14.5 and observed the effect on their development at E15.5. The expression vector for GFP (green in B, D, F, H) was also transfected together with CONsh or Cav3.2sh to detect the cells containing CONsh or Cav3.2sh. Arrowheads indicate GFP/Pax6 double-positive cells (A, B, E, F) or GFP/Tbr1 double-positive cells (C, D, G, H), and arrows indicate GFP-positive/Pax6-negative (A, B, E, F) or Tbr1-negative cells (C, D, G, H). At 24 h after the transfection, almost half of the cells were Pax6-positive (magenta in A, B), and the other half were Tbr1-positive (magenta in C, D, I). Similarly, approximately 44 % of cells containing Cav3.2sh were Pax6-positive (magenta in E, F), and 56 % were Tbr1-positive (magenta in G, H, J). (J) No significant difference was observed between GFP/Pax6 double-positive cells and GFP/Tbr1 double-positive cells per 0.031 mm^2 in Cav3.2sh. Dotted lines in (A–H) indicate the ventricular surface. Scale bar in (A) is 20 μm for (A–H). Values are mean ± SEM.

4. DISCUSSION

4.1 NPCs exhibit a distinct pattern of $[Ca^{2+}]_i$ fluctuations during development

To understand the role of $[Ca^{2+}]_i$ fluctuations in NPC differentiation, we described the pattern of spontaneous $[Ca^{2+}]_i$ fluctuations monitored by Fluo-4 AM signal during the development of self-renewing NPCs into immature neurons. We demonstrated that most cells in the VZ displayed fluctuations in the Fluo-4 AM signal in various patterns and with varying intensities (**Figure 3.3, 3.4, 3.5**). Many undifferentiated NPCs, which were defined as Pax6-positive cells, showed higher intensity of the Fluo-4 AM signal at E11, but the intensity decreased during development and toward neuronal differentiation (**Figure 3.9, 3.10, 3.11**). The number of $[Ca^{2+}]_i$ transients was low at E11 and 12, while they increased at E14 and 16 (**Figure 3.9, 3.10**). Interestingly, the number of $[Ca^{2+}]_i$ transients was higher in the differentiated neuronal cells than in NPCs (**Figure 3.11**).

Pax6 regulates the transcription of the Btg2 gene at the onset of neurogenesis by directly binding to its promoter (Sansom et al., 2009). Btg2 protein plays an important role in NPC differentiation from the self-renewing state to the neuron-generating state (Haubensak et al., 2004; Iacopetti et al., 1994; Iacopetti et al., 1999). Btg2 expression is induced by high concentration of intranuclear Ca^{2+} in cultured hippocampal neurons (Zhang et al., 2007). An increase in nuclear Ca^{2+} levels by action potential firing bursts is required for this activity-dependent regulation of Btg2 expression. Btg2 in hippocampal neurons functions as a nuclear protein involved in activity-dependent

neural survival (Zhang et al., 2007). We observed that undifferentiated Pax6-positive NPCs at E11 showed $[Ca^{2+}]_i$ fluctuations in the high $[Ca^{2+}]_i$ range (**Figure 3.9D, Figure 3.10A**). Indeed, in our experiment, it is necessary to calibrate the fluorescent Ca^{2+} indicators properly, and we realize that the intensity of Fluo-4 AM itself does not fully reflect actual $[Ca^{2+}]_i$ levels. However, from our results, we can speculate that under high $[Ca^{2+}]_i$, Pax6 may trigger the transcription of the gene that promote neuronal differentiation, causing NPCs to switch from the self-renewing state to the neurogenic state. Our finding that inhibiting $[Ca^{2+}]_i$ fluctuation inhibits neural differentiation supports this idea (**Figure 3.18A, B, C, Figure 3.19C, D, I, G, H, J**). However, further examination is still needed regarding the alteration of $[Ca^{2+}]_i$ levels that could induce the transcription of the Btg2 gene. Dragan Malic's group also found similarities in support of our hypothesis. They performed Ca^{2+} imaging on NPCs and differentiated Tuj1-positive neurons in rat embryos to investigate the cellular mechanisms involved in Ca^{2+} entry and $[Ca^{2+}]_i$ homeostasis during neurogenesis. They observed that $[Ca^{2+}]_i$ in NPCs tended to be high (>250 nM) compared to differentiated cells (50–100 nM). Although the consequence of $[Ca^{2+}]_i$ reduction in NPCs regulation remains unclear, a decrease in neuronal $[Ca^{2+}]_i$ levels correlates with the emergence of a voltage-dependent Ca^{2+} channel, which is essential for neuronal maturation (Maric et al., 2000).

The developmental role of decreased $[Ca^{2+}]_i$ described above suggests that the temporal dynamics of $[Ca^{2+}]_i$ fluctuations translate into specific effects on neuronal differentiation. This decrease in $[Ca^{2+}]_i$ may affect the role of Pax6 as a transcriptional factor during NPC development. Pax6 is expressed in both undifferentiated self-

renewing NPCs and neuron-generating NPCs and directly regulates the expression of several genes required for the differentiation of their daughter cells (Sansom et al., 2009). We observed that many of the cells showing high $[Ca^{2+}]_i$ without intermittent $[Ca^{2+}]_i$ transients were undifferentiated self-renewing Pax6-positive NPCs at E11 (**Figure 3.13A, B, E, F**), and $[Ca^{2+}]_i$ may affect their transcription by modifying the degree of chromatin compaction (Mellström & Naranjo, 2001). Under high $[Ca^{2+}]_i$ conditions, Ca^{2+}-dependent kinases phosphorylate CREB, Elk, and CBP, resulting in a low degree of chromatin compaction through phosphorylated acetylation of histone/HMG proteins, and the transcription of the genes activated by Pax6. The transcription of genes activated by Pax6 under high $[Ca^{2+}]_i$ conditions may be suppressed by the highly compacted chromatin structure under low $[Ca^{2+}]_i$ conditions. The expression of genes required for differentiation is regulated by chromosomal structure (Chen & Dent, 2014). Modification of $[Ca^{2+}]_i$ in Pax6-positive NPCs may be able to alter the gene expression profiles by altering chromatin compaction. Based on this knowledge, it may be possible to develop a technology that can control the stem cell fate by manipulating $[Ca^{2+}]_i$ or controlling the pattern of $[Ca^{2+}]_i$ fluctuation in tissue-derived stem cells using optogenetic techniques such as channel rhodopsin. Further experiments are required to establish such techniques controlling progenitor cell fate by controlling $[Ca^{2+}]_i$.

4.1.2 Number of $[Ca^{2+}]_i$ transient increases during development

More than half of Pax6-positive NPCs at E11 and E12 exhibited $[Ca^{2+}]_i$ fluctuations without any intermittent $[Ca^{2+}]_i$ transients and maintained a high $[Ca^{2+}]_i$ (**Figure 3.9C, Figure 3.10A**). On the contrary, the $[Ca^{2+}]_i$ in both Pax6-positive NPCs and immature neurons was significantly decreased at E14 and E16, whereas the number of intermittent $[Ca^{2+}]_i$ transients was increased (**Figure 3.9C, Figure 3.10A**). A previous study reported that Btg2, an antiproliferative gene expressed in neuron-generating but not self-renewing NPCs, is low at E10.5 (less than 5% VZ cell expressed Btg2) and E11.5 (less than 10%). On the other hand, it increased at E15.5 (60%; (Haubensak et al., 2004)); thus, the regulation of $[Ca^{2+}]_i$ and the intermittent $[Ca^{2+}]_i$ transients may contribute to the differentiation of self-renewing NPCs into neuron-generating NPCs or neurons (**Figure 4.1**). Furthermore, we observed that the treatment of a T-type calcium channel blocker reduced the amplitude of intermittent $[Ca^{2+}]_i$ transients (**Figure 3.16**), suggesting that voltage-gated Ca^{2+} channels regulate intermittent $[Ca^{2+}]_i$ transients. T-type Ca^{2+} channels are related to the appearance of neuronal characteristics (Kim et al., 2018). Thus, the early-stage NPCs, mostly self-renewing NPCs, may not yet express T-type Ca^{2+} channels. Therefore, it would be interesting to identify endogenous signals that trigger the expression of this Ca^{2+} channel and $[Ca^{2+}]_i$ transients in undifferentiated self-renewing Pax6-positive NPCs. In addition, further studies must identify the endogenous factors that control this signaling in developing Pax6-positive NPCs.

4.2 Role of $[Ca^{2+}]_i$ fluctuation in the proliferation and differentiation of NPCs

The findings of the current study indicated that $[Ca^{2+}]_i$ fluctuations in Pax6-positive NPCs are mediated by the T-type calcium channel (**Figure 3.16)**. Our *in vitro* and *in vivo* experiments demonstrated that the inhibition of Cav3.1, one of the three subtypes of T-type calcium channels resulted in the maintenance of proliferation of self-renewing NPCs, but suppressed their differentiation into neurons (**Figure 3.18, Figure 3.19, Figure 4.1**). Thus, these results suggested an important role of Cav3.1 in self-renewing NPC development, especially in their differentiation during the early gestational stage. We observed that knockdown of Cav3.1 impaired neural differentiation, whereas knockdown of Cav3.2 had no effect on their proliferation and differentiation at this stage (**Figure 3.19, Figure 3.20**), suggesting that Cav3.1 plays an essential role in $[Ca^{2+}]_i$ fluctuation in Pax6-positive NPCs. Consistent with finding, abundant mRNA expression of Cav3.1, but not of Cav3.2, has been observed in the prenatal cortical neural progenitors isolated from rat embryos at E14 (Kim et al., 2018). Although no obvious embryonic phenotype has been observed in Cav3.1 knockout mice (Petrenko et al., 2007), the number of immature neurons developed from mutant adult NPCs were notably decreased in the adult hippocampal dentate gyrus, suggesting that the Cav3.1 T-type calcium channel is crucial for the neural differentiation or maturation during adult hippocampal neurogenesis (Kim & Shin, 2021; Yabuki et al., 2021). Taken together, these findings suggested that the generation of $[Ca^{2+}]_i$ fluctuations by the Cav3.1 T-type calcium channel may function importantly both in in prenatal and adult neurogenesis.

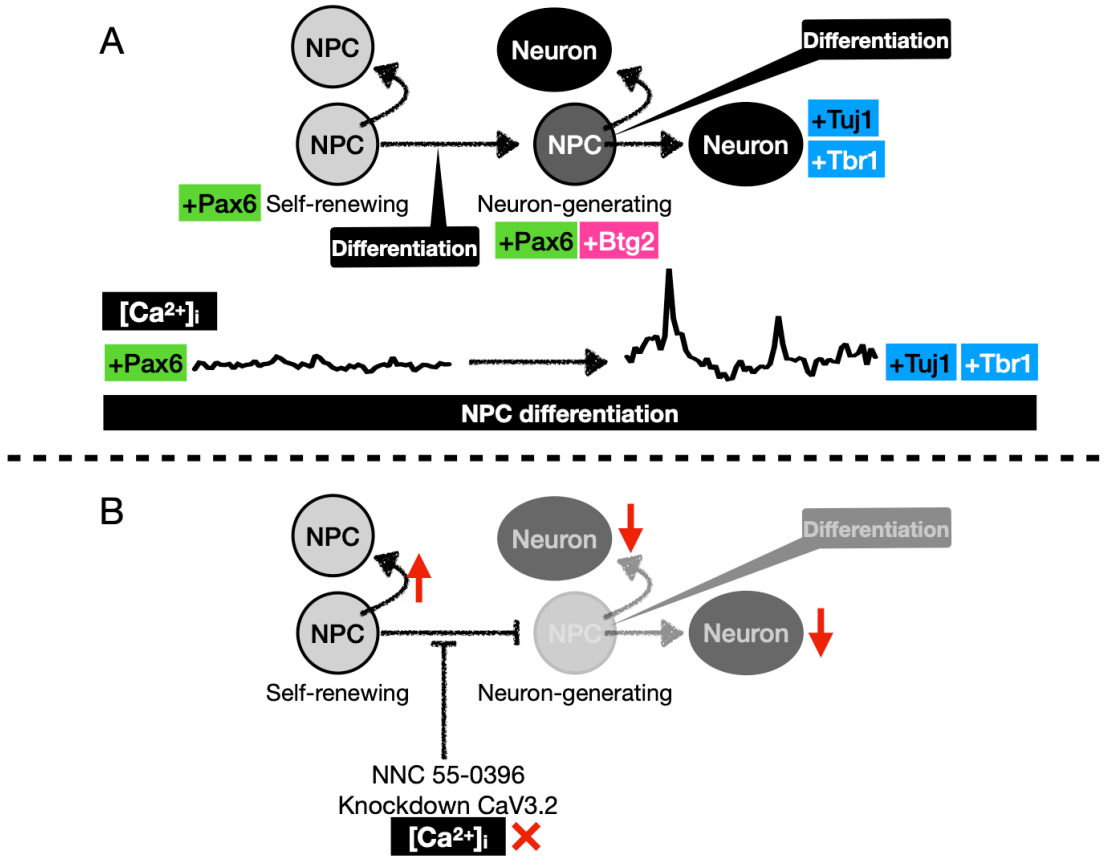

Figure 4.1. Summary.

(A) NPCs exhibit a distinct pattern of $[Ca^{2+}]_i$ fluctuations during differentiation. The number of cells displaying intermittent $[Ca^{2+}]_i$ transients in Pax6+/Btg2- NPC is significantly lower than that in neuron-generating NPC (Pax6+/Btg2+) and immature neuron (Tbr1+). (B) Role of $[Ca^{2+}]_i$ fluctuation through T-type calcium channel. T-type calcium channels in self-renewing NPCs were correlated with their differentiation into neurons; NNC 55-0396 or Cav3.1 KD maintains self-renewing NPC and inhibits differentiation into Tbr1+ neurons.

5. FUTURE PERSPECTIVE

Understanding signaling molecules involved in $[Ca^{2+}]_i$ fluctuations in NPCs is essential for elucidating the mechanisms of neuronal differentiation in mammalian brain formation. Furthermore, this knowledge may also lead to understanding the etiology of pediatric brain tumors and other developmental disorders caused by the abnormal balance between self-renewal and neurogenic NPCs, as mutated NPCs or NPCs that gain "stemness" are the origin of glioblastoma (Matarredona & Pastor, 2019; Xu et al., 2021). Moreover, Ca^{2+} channels are expressed in tumor cells (Kunzelmann, 2005), and loss of control in Ca^{2+} signaling can lead to enhanced malignant behaviors in tumor cells (Wu et al., 2021).

In this study, we provide a model in which the onset of intermittent $[Ca^{2+}]_i$ transients mediated by Cav3.1 T-type calcium channels in self-renewing NPCs was correlated to their differentiation into neurons. However, several questions still remain unanswered related to intermittent $[Ca^{2+}]_i$ transients, including the cause of the intermittent $[Ca^{2+}]_i$ transients and the identification of activated transcription factors during intermittent $[Ca^{2+}]_i$ transients. Therefore, further experiments using agonists/promoters for NPC differentiation need to be carried out (i.e., BMP, Shh, Wnt, MYC proteins, integrin-associated protein, Hippocalcin, etc.), to observe the changes that occur in $[Ca^{2+}]_i$ fluctuation patterns and their gene expression profiles, as well as changes in the expression of the Ca^{2+} channels.

6. REFERENCES

Aguado, C., García-Madrona, S., Gil-Minguez, M., & Luján, R. (2016). Ontogenic Changes and Differential Localization of T-type Ca(2+) Channel Subunits Cav3.1 and Cav3.2 in Mouse Hippocampus and Cerebellum. *Front Neuroanat*, *10*, 83. https://doi.org/10.3389/fnana.2016.00083

Bedogni, F., Hodge, R. D., Elsen, G. E., Nelson, B. R., Daza, R. A., Beyer, R. P., . . . Hevner, R. F. (2010). Tbr1 regulates regional and laminar identity of postmitotic neurons in developing neocortex. *Proc Natl Acad Sci U S A*, *107*(29), 13129-13134. https://doi.org/10.1073/pnas.1002285107

Berridge, M. J., Bootman, M. D., & Lipp, P. (1998). Calcium--a life and death signal. *Nature*, *395*(6703), 645-648. https://doi.org/10.1038/27094

Buttitta, L. A., & Edgar, B. A. (2007). Mechanisms controlling cell cycle exit upon terminal differentiation. *Curr Opin Cell Biol*, *19*(6), 697-704. https://doi.org/10.1016/j.ceb.2007.10.004

Cai, L., Hayes, N. L., Takahashi, T., Caviness, V. S., & Nowakowski, R. S. (2002). Size distribution of retrovirally marked lineages matches prediction from population measurements of cell cycle behavior. *J Neurosci Res*, *69*(6), 731-744. https://doi.org/10.1002/jnr.10398

Canzoniere, D., Farioli-Vecchioli, S., Conti, F., Ciotti, M. T., Tata, A. M., Augusti-Tocco, G., . . . Tirone, F. (2004). Dual control of neurogenesis by PC3 through cell cycle inhibition and induction of Math1. *J Neurosci*, *24*(13), 3355-3369. https://doi.org/10.1523/JNEUROSCI.3860-03.2004

Catterall, W. A. (2011). Voltage-gated calcium channels. *Cold Spring Harb Perspect Biol*, *3*(8), a003947. https://doi.org/10.1101/cshperspect.a003947

Chemin, J., Nargeot, J., & Lory, P. (2002). Neuronal T-type alpha 1H calcium channels induce neuritogenesis and expression of high-voltage-activated calcium channels in the NG108-15 cell line. *J Neurosci*, *22*(16), 6856-6862. https://doi.org/20026671

Chen, T., & Dent, S. Y. (2014). Chromatin modifiers and remodellers: regulators of cellular differentiation. *Nat Rev Genet*, *15*(2), 93-106. https://doi.org/10.1038/nrg3607

Chiasson, B. J., Tropepe, V., Morshead, C. M., & van der Kooy, D. (1999). Adult mammalian forebrain ependymal and subependymal cells demonstrate proliferative potential, but only subependymal cells have neural stem cell characteristics. *J Neurosci*, *19*(11), 4462-4471.

De Robertis, E. M., & Kuroda, H. (2004). Dorsal-ventral patterning and neural induction in Xenopus embryos. *Annu Rev Cell Dev Biol*, *20*, 285-308. https://doi.org/10.1146/annurev.cellbio.20.011403.154124

Draganova, K., Zemke, M., Zurkirchen, L., Valenta, T., Cantù, C., Okoniewski, M., . . . Sommer, L. (2015). Wnt/β-catenin signaling regulates sequential fate decisions of murine cortical precursor cells. *Stem Cells*, *33*(1), 170-182. https://doi.org/10.1002/stem.1820

Eckenhoff, M. F., & Rakic, P. (1988). Nature and fate of proliferative cells in the hippocampal dentate gyrus during the life span of the rhesus monkey. *J Neurosci*, *8*(8), 2729-2747.

Englund, C., Fink, A., Lau, C., Pham, D., Daza, R. A., Bulfone, A., . . . Hevner, R. F. (2005). Pax6, Tbr2, and Tbr1 are expressed sequentially by radial glia, intermediate progenitor cells, and postmitotic neurons in developing neocortex. *J Neurosci*, *25*(1), 247-251. https://doi.org/10.1523/JNEUROSCI.2899-04.2005

Estivill-Torrus, G., Pearson, H., van Heyningen, V., Price, D. J., & Rashbass, P. (2002). Pax6 is required to regulate the cell cycle and the rate of progression from symmetrical to asymmetrical division in mammalian cortical progenitors. *Development*, *129*(2), 455-466.

Farioli-Vecchioli, S., Saraulli, D., Costanzi, M., Leonardi, L., Cinà, I., Micheli, L., . . . Tirone, F. (2009). Impaired terminal differentiation of hippocampal granule neurons and defective contextual memory in PC3/Tis21 knockout mice. *PLoS One*, *4*(12), e8339. https://doi.org/10.1371/journal.pone.0008339

Farioli-Vecchioli, S., Saraulli, D., Costanzi, M., Pacioni, S., Cinà, I., Aceti, M., . . . Tirone, F. (2008). The timing of differentiation of adult hippocampal neurons is crucial for spatial memory. *PLoS Biol*, *6*(10), e246. https://doi.org/10.1371/journal.pbio.0060246

Farioli-Vecchioli, S., Tanori, M., Micheli, L., Mancuso, M., Leonardi, L., Saran, A., . . . Tirone, F. (2007). Inhibition of medulloblastoma tumorigenesis by the antiproliferative and pro-differentiative gene PC3. *FASEB J*, *21*(9), 2215-2225. https://doi.org/10.1096/fj.06-7548com

Ferrari, M. B., Rohrbough, J., & Spitzer, N. C. (1996). Spontaneous calcium transients regulate myofibrillogenesis in embryonic Xenopus myocytes. *Dev Biol*, *178*(2), 484-497. https://doi.org/10.1006/dbio.1996.0233

Fishell, G., & Kriegstein, A. R. (2003). Neurons from radial glia: the consequences of asymmetric inheritance. *Curr Opin Neurobiol*, *13*(1), 34-41. https://doi.org/10.1016/s0959-4388(03)00013-8

Gan, Q., Lee, A., Suzuki, R., Yamagami, T., Stokes, A., Nguyen, B. C., . . . Zhou, C. J. (2014). Pax6 mediates ß-catenin signaling for self-renewal and neurogenesis by neocortical radial glial stem cells. *Stem Cells*, *32*(1), 45-58. https://doi.org/10.1002/stem.1561

Götz, M., & Huttner, W. B. (2005). The cell biology of neurogenesis. *Nat Rev Mol Cell Biol*, *6*(10), 777-788. https://doi.org/10.1038/nrm1739

Haubensak, W., Attardo, A., Denk, W., & Huttner, W. B. (2004). Neurons arise in the basal neuroepithelium of the early mammalian telencephalon: a major site of neurogenesis. *Proc Natl Acad Sci U S A*, *101*(9), 3196-3201. https://doi.org/10.1073/pnas.0308600100

Heins, N., Malatesta, P., Cecconi, F., Nakafuku, M., Tucker, K. L., Hack, M. A., . . . Götz, M. (2002). Glial cells generate neurons: the role of the transcription factor Pax6. *Nat Neurosci*, *5*(4), 308-315. https://doi.org/10.1038/nn828

Hitoshi, S., Seaberg, R. M., Koscik, C., Alexson, T., Kusunoki, S., Kanazawa, I., . . . van der Kooy, D. (2004). Primitive neural stem cells from the mammalian epiblast differentiate to definitive neural stem cells under the control of Notch signaling. *Genes Dev*, *18*(15), 1806-1811. https://doi.org/10.1101/gad.1208404

Horton, A. R., & Davies, A. M. (2020). Initial axon growth rate from embryonic sensory neurons is correlated with birth date. *Dev Neurobiol*, *80*(3-4), 126-131. https://doi.org/10.1002/dneu.22743

Huang, L., Keyser, B. M., Tagmose, T. M., Hansen, J. B., Taylor, J. T., Zhuang, H., . . . Li, M. (2004). NNC 55-0396 [(1S,2S)-2-(2-(N-[(3-benzimidazol-2-yl)propyl]-N-

methylamino)ethyl)-6-fluoro-1,2,3,4-tetrahydro-1-isopropyl-2-naphtyl cyclopropanecarboxylate dihydrochloride]: a new selective inhibitor of T-type calcium channels. *J Pharmacol Exp Ther*, *309*(1), 193-199. https://doi.org/10.1124/jpet.103.060814

Iacopetti, P., Barsacchi, G., Tirone, F., Maffei, L., & Cremisi, F. (1994). Developmental expression of PC3 gene is correlated with neuronal cell birthday. *Mech Dev*, *47*(2), 127-137. https://doi.org/10.1016/0925-4773(94)90085-x

Iacopetti, P., Michelini, M., Stuckmann, I., Oback, B., Aaku-Saraste, E., & Huttner, W. B. (1999). Expression of the antiproliferative gene TIS21 at the onset of neurogenesis identifies single neuroepithelial cells that switch from proliferative to neuron-generating division. *Proc Natl Acad Sci U S A*, *96*(8), 4639-4644. https://doi.org/10.1073/pnas.96.8.4639

Kang, S., Chen, X., Gong, S., Yu, P., Yau, S., Su, Z., . . . Shi, L. (2017). Characteristic analyses of a neural differentiation model from iPSC-derived neuron according to morphology, physiology, and global gene expression pattern. *Sci Rep*, *7*(1), 12233. https://doi.org/10.1038/s41598-017-12452-x

Kapur, N., Mignery, G. A., & Banach, K. (2007). Cell cycle-dependent calcium oscillations in mouse embryonic stem cells. *Am J Physiol Cell Physiol*, *292*(4), C1510-1518. https://doi.org/10.1152/ajpcell.00181.2006

Kawaguchi, A., Miyata, T., Sawamoto, K., Takashita, N., Murayama, A., Akamatsu, W., . . . Okano, H. (2001). Nestin-EGFP transgenic mice: visualization of the self-renewal and multipotency of CNS stem cells. *Mol Cell Neurosci*, *17*(2), 259-273. https://doi.org/10.1006/mcne.2000.0925

Kawano, S., Shoji, S., Ichinose, S., Yamagata, K., Tagami, M., & Hiraoka, M. (2002). Characterization of Ca(2+) signaling pathways in human mesenchymal stem cells. *Cell Calcium*, *32*(4), 165-174. https://doi.org/10.1016/s0143416002001240

Kim, J. W., Oh, H. A., Kim, S. R., Ko, M. J., Seung, H., Lee, S. H., & Shin, C. Y. (2020). Epigenetically Upregulated T-Type Calcium Channels Contribute to Abnormal Proliferation of Embryonic Neural Progenitor Cells Exposed to Valproic Acid. *Biomol Ther (Seoul)*, *28*(5), 389-396. https://doi.org/10.4062/biomolther.2020.027

Kim, J. W., Oh, H. A., Lee, S. H., Kim, K. C., Eun, P. H., Ko, M. J., . . . Shin, C. Y. (2018). T-Type Calcium Channels Are Required to Maintain Viability of Neural Progenitor Cells. *Biomol Ther (Seoul)*, *26*(5), 439-445. https://doi.org/10.4062/biomolther.2017.223

Kim, J. W., & Shin, C. Y. (2021). Deciphering the role of T-type calcium channels in regulating adult hippocampal neurogenesis. *Acta Physiol (Oxf)*, *232*(1), e13643. https://doi.org/10.1111/apha.13643

Kraft, A., Jubal, E. R., von Laer, R., Döring, C., Rocha, A., Grebbin, M., . . . Momma, S. (2017). Astrocytic Calcium Waves Signal Brain Injury to Neural Stem and Progenitor Cells. *Stem Cell Reports*, *8*(3), 701-714. https://doi.org/10.1016/j.stemcr.2017.01.009

Kraft, R. (2015). STIM and ORAI proteins in the nervous system. *Channels (Austin)*, *9*(5), 245-252. https://doi.org/10.1080/19336950.2015.1071747

Kunzelmann, K. (2005). Ion channels and cancer. *J Membr Biol*, *205*(3), 159-173. https://doi.org/10.1007/s00232-005-0781-4

Lamb, T. M., & Harland, R. M. (1995). Fibroblast growth factor is a direct neural inducer, which combined with noggin generates anterior-posterior neural pattern. *Development*, *121*(11), 3627-3636. https://doi.org/10.1242/dev.121.11.3627

Leclerc, C., Daguzan, C., Nicolas, M. T., Chabret, C., Duprat, A. M., & Moreau, M. (1997). L-type calcium channel activation controls the in vivo transduction of the neuralizing signal in the amphibian embryos. *Mech Dev*, *64*(1-2), 105-110. https://doi.org/10.1016/s0925-4773(97)00054-3

Leclerc, C., Rizzo, C., Daguzan, C., Néant, I., Batut, J., Augé, B., & Moreau, M. (2001). [Neural determination in Xenopus laevis embryos: control of early neural gene expression by calcium]. *J Soc Biol*, *195*(3), 327-337.

Leclerc, C., Webb, S. E., Daguzan, C., Moreau, M., & Miller, A. L. (2000). Imaging patterns of calcium transients during neural induction in Xenopus laevis embryos. *J Cell Sci*, *113 Pt 19*, 3519-3529. https://doi.org/10.1242/jcs.113.19.3519

Lepski, G., Jannes, C. E., Nikkhah, G., & Bischofberger, J. (2013). cAMP promotes the differentiation of neural progenitor cells in vitro via modulation of voltage-gated calcium channels. *Front Cell Neurosci*, *7*, 155. https://doi.org/10.3389/fncel.2013.00155

Liu, X., Hashimoto-Torii, K., Torii, M., Haydar, T. F., & Rakic, P. (2008). The role of ATP signaling in the migration of intermediate neuronal progenitors to the neocortical subventricular zone. *Proc Natl Acad Sci U S A*, *105*(33), 11802-11807. https://doi.org/10.1073/pnas.0805180105

LoTurco, J. J., Owens, D. F., Heath, M. J., Davis, M. B., & Kriegstein, A. R. (1995). GABA and glutamate depolarize cortical progenitor cells and inhibit DNA synthesis. *Neuron*, *15*(6), 1287-1298. https://doi.org/10.1016/0896-6273(95)90008-x

Luhmann, H. J., Sinning, A., Yang, J. W., Reyes-Puerta, V., Stüttgen, M. C., Kirischuk, S., & Kilb, W. (2016). Spontaneous Neuronal Activity in Developing Neocortical Networks: From Single Cells to Large-Scale Interactions. *Front Neural Circuits*, *10*, 40. https://doi.org/10.3389/fncir.2016.00040

Malmersjö, S., Rebellato, P., Smedler, E., Planert, H., Kanatani, S., Liste, I., . . . Uhlén, P. (2013). Neural progenitors organize in small-world networks to promote cell proliferation. *Proc Natl Acad Sci U S A*, *110*(16), E1524-1532. https://doi.org/10.1073/pnas.1220179110

Maric, D., Maric, I., & Barker, J. L. (2000). Developmental changes in cell calcium homeostasis during neurogenesis of the embryonic rat cerebral cortex. *Cereb Cortex*, *10*(6), 561-573. https://doi.org/10.1093/cercor/10.6.561

Martin, R. L., Lee, J. H., Cribbs, L. L., Perez-Reyes, E., & Hanck, D. A. (2000). Mibefradil block of cloned T-type calcium channels. *J Pharmacol Exp Ther*, *295*(1), 302-308.

Masnadi-Shirazi, M., Maurya, M. R., Pao, G., Ke, E., Verma, I. M., & Subramaniam, S. (2019). Time varying causal network reconstruction of a mouse cell cycle. *BMC Bioinformatics*, *20*(1), 294. https://doi.org/10.1186/s12859-019-2895-1

Matarredona, E. R., & Pastor, A. M. (2019). Neural Stem Cells of the Subventricular Zone as the Origin of Human Glioblastoma Stem Cells. Therapeutic Implications. *Front Oncol*, *9*, 779. https://doi.org/10.3389/fonc.2019.00779

Mellström, B., & Naranjo, J. R. (2001). Mechanisms of Ca(2+)-dependent transcription. *Curr Opin Neurobiol*, *11*(3), 312-319. https://doi.org/10.1016/s0959-4388(00)00213-0

Moreau, M., Leclerc, C., Gualandris-Parisot, L., & Duprat, A. M. (1994). Increased internal Ca2+ mediates neural induction in the amphibian embryo. *Proc Natl Acad Sci U S A*, *91*(26), 12639-12643. https://doi.org/10.1073/pnas.91.26.12639

Murphy, T. H., Blatter, L. A., Wier, W. G., & Baraban, J. M. (1992). Spontaneous synchronous synaptic calcium transients in cultured cortical neurons. *J Neurosci*, *12*(12), 4834-4845.

Noctor, S. C., Martínez-Cerdeño, V., Ivic, L., & Kriegstein, A. R. (2004). Cortical neurons arise in symmetric and asymmetric division zones and migrate through specific phases. *Nat Neurosci*, *7*(2), 136-144. https://doi.org/10.1038/nn1172

Owens, D. F., & Kriegstein, A. R. (1998). Patterns of intracellular calcium fluctuation in precursor cells of the neocortical ventricular zone. *J Neurosci*, *18*(14), 5374-5388.

Petrenko, A. B., Tsujita, M., Kohno, T., Sakimura, K., & Baba, H. (2007). Mutation of alpha1G T-type calcium channels in mice does not change anesthetic requirements for loss of the righting reflex and minimum alveolar concentration but delays the onset of anesthetic induction. *Anesthesiology*, *106*(6), 1177-1185. https://doi.org/10.1097/01.anes.0000267601.09764.e6

Qian, X., Shen, Q., Goderie, S. K., He, W., Capela, A., Davis, A. A., & Temple, S. (2000). Timing of CNS cell generation: a programmed sequence of neuron and glial cell production from isolated murine cortical stem cells. *Neuron*, *28*(1), 69-80. https://doi.org/10.1016/s0896-6273(00)00086-6

Quinn, J. C., Molinek, M., Martynoga, B. S., Zaki, P. A., Faedo, A., Bulfone, A., . . . Price, D. J. (2007). Pax6 controls cerebral cortical cell number by regulating exit from the cell cycle and specifies cortical cell identity by a cell autonomous mechanism. *Dev Biol*, *302*(1), 50-65. https://doi.org/10.1016/j.ydbio.2006.08.035

Rash, B. G., Ackman, J. B., & Rakic, P. (2016). Bidirectional radial Ca(2+) activity regulates neurogenesis and migration during early cortical column formation. *Sci Adv*, *2*(2), e1501733. https://doi.org/10.1126/sciadv.1501733

Rodríguez-Gómez, J. A., Levitsky, K. L., & López-Barneo, J. (2012). T-type Ca2+ channels in mouse embryonic stem cells: modulation during cell cycle and contribution to self-renewal. *Am J Physiol Cell Physiol*, *302*(3), C494-504. https://doi.org/10.1152/ajpcell.00267.2011

Rosenberg, S. S., & Spitzer, N. C. (2011). Calcium signaling in neuronal development. *Cold Spring Harb Perspect Biol*, *3*(10), a004259. https://doi.org/10.1101/cshperspect.a004259

Sansom, S. N., Griffiths, D. S., Faedo, A., Kleinjan, D. J., Ruan, Y., Smith, J., . . . Livesey, F. J. (2009). The level of the transcription factor Pax6 is essential for controlling the balance between neural stem cell self-renewal and neurogenesis. *PLoS Genet*, *5*(6), e1000511. https://doi.org/10.1371/journal.pgen.1000511

Schwirtlich, M., Emri, Z., Antal, K., Máté, Z., Katarova, Z., & Szabó, G. (2010). GABA(A) and GABA(B) receptors of distinct properties affect oppositely the proliferation of mouse embryonic stem cells through synergistic elevation of intracellular Ca(2+). *FASEB J*, *24*(4), 1218-1228. https://doi.org/10.1096/fj.09-143586

Shi, Y., Sun, G., Zhao, C., & Stewart, R. (2008). Neural stem cell self-renewal. *Crit Rev Oncol Hematol*, *65*(1), 43-53. https://doi.org/10.1016/j.critrevonc.2007.06.004

Solozobova, V., Wyvekens, N., & Pruszak, J. (2012). Lessons from the embryonic neural stem cell niche for neural lineage differentiation of pluripotent stem cells. *Stem Cell Rev Rep*, *8*(3), 813-829. https://doi.org/10.1007/s12015-012-9381-8

Sperelakis, N., Tohse, N., Ohya, Y., & Masuda, H. (1994). Cyclic GMP regulation of calcium slow channels in cardiac muscle and vascular smooth muscle cells. *Adv Pharmacol*, *26*, 217-252. https://doi.org/10.1016/s1054-3589(08)60056-3

Suzuki, M., Sato, M., Koyama, H., Hara, Y., Hayashi, K., Yasue, N., . . . Ueno, N. (2017). Distinct intracellular Ca. *Development*, *144*(7), 1307-1316. https://doi.org/10.1242/dev.141952

Tabata, H., & Nakajima, K. (2001). Efficient in utero gene transfer system to the developing mouse brain using electroporation: visualization of neuronal migration in the developing cortex. *Neuroscience*, *103*(4), 865-872. https://doi.org/10.1016/s0306-4522(01)00016-1

Takahashi, T., Nowakowski, R. S., & Caviness, V. S. (1995). The cell cycle of the pseudostratified ventricular epithelium of the embryonic murine cerebral wall. *J Neurosci*, *15*(9), 6046-6057.

Taylor, J. T., Huang, L., Pottle, J. E., Liu, K., Yang, Y., Zeng, X., . . . Li, M. (2008). Selective blockade of T-type Ca2+ channels suppresses human breast cancer cell proliferation. *Cancer Lett*, *267*(1), 116-124. https://doi.org/10.1016/j.canlet.2008.03.032

Tonelli, F. M., Santos, A. K., Gomes, D. A., da Silva, S. L., Gomes, K. N., Ladeira, L. O., & Resende, R. R. (2012). Stem cells and calcium signaling. *Adv Exp Med Biol*, *740*, 891-916. https://doi.org/10.1007/978-94-007-2888-2_40

Tsai, F. C., Kuo, G. H., Chang, S. W., & Tsai, P. J. (2015). Ca2+ signaling in cytoskeletal reorganization, cell migration, and cancer metastasis. *Biomed Res Int*, *2015*, 409245. https://doi.org/10.1155/2015/409245

Uhlén, P., & Fritz, N. (2010). Biochemistry of calcium oscillations. *Biochem Biophys Res Commun*, *396*(1), 28-32. https://doi.org/10.1016/j.bbrc.2010.02.117

Vandecasteele, G., Verde, I., Rücker-Martin, C., Donzeau-Gouge, P., & Fischmeister, R. (2001). Cyclic GMP regulation of the L-type Ca(2+) channel current in human atrial myocytes. *J Physiol*, *533*(Pt 2), 329-340. https://doi.org/10.1111/j.1469-7793.2001.0329a.x

Vescovi, A. L., & Snyder, E. Y. (1999). Establishment and properties of neural stem cell clones: plasticity in vitro and in vivo. *Brain Pathol*, *9*(3), 569-598. https://doi.org/10.1111/j.1750-3639.1999.tb00542.x

Webb, S. E., & Miller, A. L. (2003). Calcium signalling during embryonic development. *Nat Rev Mol Cell Biol*, *4*(7), 539-551. https://doi.org/10.1038/nrm1149

Weiss, S., Dunne, C., Hewson, J., Wohl, C., Wheatley, M., Peterson, A. C., & Reynolds, B. A. (1996). Multipotent CNS stem cells are present in the adult mammalian spinal cord and ventricular neuroaxis. *J Neurosci*, *16*(23), 7599-7609.

Weissman, T. A., Riquelme, P. A., Ivic, L., Flint, A. C., & Kriegstein, A. R. (2004). Calcium waves propagate through radial glial cells and modulate proliferation in the developing neocortex. *Neuron*, *43*(5), 647-661. https://doi.org/10.1016/j.neuron.2004.08.015

Woodhead, G. J., Mutch, C. A., Olson, E. C., & Chenn, A. (2006). Cell-autonomous beta-catenin signaling regulates cortical precursor proliferation. *J Neurosci*, *26*(48), 12620-12630. https://doi.org/10.1523/JNEUROSCI.3180-06.2006

Wu, L., Lian, W., & Zhao, L. (2021). Calcium signaling in cancer progression and therapy. *FEBS J*, *288*(21), 6187-6205. https://doi.org/10.1111/febs.16133

Xu, L., Zhang, M., Shi, L., Yang, X., Chen, L., Cao, N., . . . Cao, Y. (2021). Neural stemness contributes to cell tumorigenicity. *Cell Biosci*, *11*(1), 21. https://doi.org/10.1186/s13578-021-00531-6

Yabuki, Y., Matsuo, K., Yu, M., Xu, J., Sakimura, K., Shioda, N., & Fukunaga, K. (2021). Cav3.1 t-type calcium channel is critical for cell proliferation and survival in newly generated

cells of the adult hippocampus. *Acta Physiol (Oxf)*, *232*(1), e13613. https://doi.org/10.1111/apha.13613

Yunker, A. M., Sharp, A. H., Sundarraj, S., Ranganathan, V., Copeland, T. D., & McEnery, M. W. (2003). Immunological characterization of T-type voltage-dependent calcium channel CaV3.1 (alpha 1G) and CaV3.3 (alpha 1I) isoforms reveal differences in their localization, expression, and neural development. *Neuroscience*, *117*(2), 321-335. https://doi.org/10.1016/s0306-4522(02)00936-3

Yuryev, M., Andriichuk, L., Leiwe, M., Jokinen, V., Carabalona, A., & Rivera, C. (2018). In vivo two-photon imaging of the embryonic cortex reveals spontaneous ketamine-sensitive calcium activity. *Sci Rep*, *8*(1), 16059. https://doi.org/10.1038/s41598-018-34410-x

Yuryev, M., Pellegrino, C., Jokinen, V., Andriichuk, L., Khirug, S., Khiroug, L., & Rivera, C. (2015). In vivo Calcium Imaging of Evoked Calcium Waves in the Embryonic Cortex. *Front Cell Neurosci*, *9*, 500. https://doi.org/10.3389/fncel.2015.00500

Zhang, S. J., Steijaert, M. N., Lau, D., Schütz, G., Delucinge-Vivier, C., Descombes, P., & Bading, H. (2007). Decoding NMDA receptor signaling: identification of genomic programs specifying neuronal survival and death. *Neuron*, *53*(4), 549-562. https://doi.org/10.1016/j.neuron.2007.01.025